Systemic 4-1BB stimulation augments extrafollicular memory B cell formation and recall responses during *Plasmodium* infection.

Carolina Caloba[1,2,3], Alexandria J. Sturtz[4], Taylor A. Lyons[3], Lijo John[1,5], Akshaya Ramachandran[1,2], Allen M. Minns[6], Anthony M. Cannon[7], Justin P. Whalley[1,3], Tania H. Watts[8], Mark H. Kaplan[7], Scott E. Lindner[5], Rahul Vijay[1,3]

[1]Discipline of Microbiology and Immunology, [2]School of Graduate and Postdoctoral Studies, [3] Center for Cancer Biology, Immunology and Infection, Rosalind Franklin University of Medicine and Science, North Chicago, IL, USA. [4]Division of Biology and Biomedical Sciences, Washington University, St. Louis, Missouri, USA. [5]Deparment of Veterinary Biochemistry, Kerala Veterinary and Animal Sciences University, Kerala, India. [6]Department of Biochemistry and Molecular Biology, Huck Center for Malaria Research, Pennsylvania State University, University Park, Pennsylvania, USA. [7]Department of Microbiology and Immunology, Indiana University School of Medicine, Indianapolis, IN, USA. [8]Department of Immunology, Temerty Faculty of Medicine, University of Toronto, Toronto, ON, Canada.

Running Title: 4-1BB stimulation and memory B cells in malaria

Summary:

T-dependent germinal center (GC) output, comprising plasma cells (PC) and memory B cells (MBC), is crucial for the clearance of *Plasmodium* infection and protection against reinfection. In this study, we examined the effect of an agonistic antibody targeting 4-1BB (CD137), a member of the Tumor Necrosis Factor Receptor Superfamily (TNFRSF), during experimental malaria. Here we show that exogenous 4-1BB stimulation, despite delaying the effector GC response, surprisingly enhanced humoral memory recall and protection from reinfection. Single cell RNA and ATAC sequencing of MBCs from mice that received 4-1BB stimulation revealed distinct populations with transcriptional and epigenetic signatures indicative of superior recall and proliferative potential. Importantly, our results indicate that the effects of 4-1BB stimulation are dependent on IL-9R signaling in B cells but independent of parasite load during primary infection. Our study proposes an immunomodulatory approach to enhance the quality of the MBC pool, providing superior protection during infection and vaccination, particularly in the context of malaria.

Introduction

Despite decades of research, malaria remains a major public health threat, with an estimated 249 million cases and 608,000 deaths in 2022[1]. It predominantly affects poorer regions, with almost 95% of cases and 98% of deaths documented in Africa. The severity of the disease is especially prominent in individuals with limited or no prior exposure to the parasite, making children under the age of 5 the most impacted[1,2]. The newly approved anti-malarial vaccines RTS,S/AS01 and R21 provide waning efficacy even after a multi-dose regimen[3]. Clearance of the malarial parasite relies on CD4 T cell-dependent B cell activation, culminating in the production of parasite-specific antibodies during the blood stage of infection[4,5]. Prior to or concomitant with the clearance of infection, a fraction of activated B cells differentiates into memory B cells (MBCs) which quickly become antibody-secreting plasma cells (PCs) upon reinfection[6-11,12]. However, increasing evidence suggests that even after multiple exposures, naturally acquired anti-*Plasmodium* humoral immune memory affords just clinical immunity and not sterilizing immunity, resulting in repeat infections[13].

Leveraging numerous studies in tumor models, the expression and engagement of coinhibitory receptors such as PD-1, LAG-3, and CTLA-4 on CD4 T cells have been identified as contributing to the inefficient anti-*Plasmodium* immune responses [14-18]. In one such study, exogenous

activation of OX40, a member of the tumor necrosis factor receptor superfamily (TNFRSF) expressed on T cells improved *Plasmodium* clearance following primary infection and also rendered protection from rechallenge in a model of experimental malaria [16,17]. These studies highlight substantial room for improvement in the natural immune response against *Plasmodium* and underscore the potential of exogenous costimulatory agonists to fully harness the full breadth of the immune system.

4-1BB (CD137), another TNFRSF member predominantly expressed on T cells, has been shown to have non-redundant roles with OX40 in enhancing CD4 T cell function[19,20]. Given that CD4 T cells play a key role in anti-*Plasmodium* immunity by providing help to B cells, we investigated the role of exogenous 4-1BB stimulation in a rodent malaria model. Here, we show that exogenous ligation of 4-1BB using a monoclonal antibody significantly delayed the effector humoral response while paradoxically enhancing humoral immune memory. Transcriptomic and epigenetic analysis of MBCs from treated mice suggests they have a distinct genetic signature that facilitate superior recall and strongly points to an extrafollicular origin. Additionally, this enhanced protection following 4-1BB activation depended on IFNγ-induced expression of T-BET in B cells during the effector phase and, more importantly, IL-9:IL-9R signaling on MBCs. Collectively, our study establishes a previously unidentified pathway by which MBCs can be programmed to attain superior recall potential and identify key molecules that may be targeted to enhance vaccine efficacy especially in *Plasmodium* infections.

Materials and Methods

Animals, infection, treatments and parasitemia

C57BL/6 mice and *Tbx21*$^{-/-}$ mice were purchased from The Jackson Laboratory. 4-1BB$^{-/-}$ mice were originally obtained from Byoug S. Kwon, Korean National University[21] and transferred to THW and RV labs for these studies. *Plasmodium yoelli* (*Py*) clone 17XNL and *P. berghei* clone ANKA (*PbA*) were obtained from the Malaria Research and Reference Reagent Resource Center (MR4; American Type Culture Collection), stocks generated and mice infected as previously described[22]. Briefly, frozen parasite stocks (200μL aliquots) were resuspended in 4mL of normal saline or PBS (1:20 dilution) and animals were infected with 1x10^6 parasitized RBCs intravenously. Treatments with all biologics were done intraperitoneally in a 200μL volume (in PBS) as follows: 50 μg of anti-4-1BB antibody (3H3; BioXCell), 200μg of IFNγ blocking antibody (XMG1.2; Bioxcell), 100μg IL-9 blocking antibody (9C1; Bioxcell) or rat IgG (rIgG) or mouse IgG (mIgG) on indicated timepoints. Mice were treated with artemether (Biotechne) at 20mg/kg, dissolved in 50μL of mineral oil at indicated timepoints. Parasitemia was measured by flow cytometry as previously described[23,24]. All experiments and procedures were approved by the Rosalind Franklin University of Medicine and Science Institutional Animal Care and Use Committee.

Competitive mixed bone marrow chimeras

C57BL/6 mice (CD45.1/.1) were lethally irradiated (950 rads) and transferred with 10x10^6 cells containing a mixture of μMT cells (CD45.1/.2) along with *Tbx21*$^{-/-}$ (CD45.2/.2) or *Il9r*$^{-/-}$ (CD45.2/.2) or WT (CD45.2/.2) cells at an 8:2 ratio, respectively. For CD4-specific competitive mixed bone marrow chimeras, TCRα$^{-/-}$ were used as recipients and transferred with 10x10^6 cells of CD4$^{-/-}$ cells (CD45.2/CD45.2) along with *4*-1BB$^{-/-}$ (CD45.1/.1) or WT (CD45.1/.1) cells at an 8:2 ratio, respectively. At 6 weeks post transfer mice were checked for reconstitution (>90% donor; 80%

μMT or TCRα cells and 10% KO cells) by flow cytometry and at 8 weeks post transfer, reconstituted mice were used for the experiments listed elsewhere.

Confocal imaging

Spleens were processed as previously described[22]. Antibodies used for staining are B220-AF488 (clone RA3-6B2; eBioscience), CD4-AF594 (clone GK1.5; BioLegend) and GL7-AF647 (BD Pharmingen). Imaging was done using a Zeiss LSM710 confocal microscope and images were processed using IMARIS x64 software (version 9.2.1).

ELISpot and ELISA

For ELISPOT, Nunc MaxiSorp white polystyrene plates were coated with 0.5 μg ml^{-1} of recombinant $MSP1_{19}$ and blocked for at least 2 h with supplemented Roswell Park Memorial Institute (RPMI) 1640 media. Bone marrow cells from *PbA*-infected mice were serially diluted in supplemented RPMI 1640 media and plated for 20 h at 37 °C with 5% CO_2. Plates were washed with PBS + 0.05% Tween 20 and incubated overnight with horseradish peroxidase (HRP)-conjugated IgM at 4 °C. Spots were developed with 3-amino-9-ethylcarbazole.
For ELISA, Nunc MaxiSorp plates were coated with 0.5 μg ml^{-1} $MSP1_{19}$ and blocked with 2.5% w/v BSA + 5% v/v fetal bovine serum. Serum samples from naive and *Py*-infected mice were serially diluted and incubated for 18 h at 4 °C. $MSP1_{19}$-specific antibodies were detected with HRP-conjugated IgM, IgG2b or IgG2c at 1:1000 dilution. Plates were developed using a SureBlue reserve TMB Kit (KPL), according to the manufacturer's protocol, and absorbance was measured at an optical density of 450 nm using a Accuris ELISA plate reader. End-point titers were extrapolated from a sigmoidal 4PL (where x is the log concentration) standard curve for each sample. The threshold for end-point titers was the mean plus 0.5–8 multiplied by the standard deviation recorded for naive mouse sera.

Ex vivo B cell activation

Splenic cells were enriched for B cells using the MojoSort™ Mouse Pan B Cell Isolation Kit (Biolegend) according to the manufacturer's protocol. 7.5 x10^5 B cells were plated in triplicates and were activated with anti-IgM (10μg/mL) and anti-CD40 (10μg/mL). Some wells received rIFNγ (20ng/mL).

Intracellular cytokine stimulation

Single cell suspension of splenocytes were prepared and 1x 10^6 were seeded in U-bottom wells in 96-well plate. The cells were stimulated with cell activation cocktail (BioLegend) containing phorbol myristate acetate (PMA) and Ionomycin in the presence of brefeldin A (BioLegend) for 4 hours at 37°C and 5% CO_2. After incubation, cells were stained as described elsewhere in the manuscript.

SpyCage Reagent for detecting and enriching $MSP1_{-19}$ specific B cells

SpyCage reagents bearing 60 copies of either mScarlet ("RedCage") or mNeonGreen ("GreenCage") were covalently loaded with 60 copies of the immunodominant *P. yoelii* antigen MSP-1 or the liver stage antigen *Py*UIS4 as a decoy control, respectively. Antibodies specific to SpyCage were biotinylated using amine-reactive biotinylated crosslinkers and were used to enrich

SpyCage-bound cells[25]. Briefly, single cell suspensions were stained with 1.25mg of *Py*UIS4 for 10 minutes at room temperature followed by *Py*MSP-1 (1.25mg) staining for 30 minutes at 4°C. Cells were washed and incubated with 1mg of anti-aldolase biotynilated antibody for 30 minutes at 4°C. Stained cells were then washed and enriched with MojoSort™ Streptavidin nanobeads (Biolegend), according to the manufacturer's protocol. Enriched cells were used for surface and intranuclear staining as detailed below.

Flow cytometry

Spleens were harvested and homogenized through wire meshes to obtain single cell suspensions. After RBCs lysis, cells were filtered and counted. Samples were blocked using Fc block (clone 2.4G2) in FACS buffer (PBS + 0.002% w/v sodium azide + 2% v/v fetal bovine serum) and cells were stained with fluorescently labeled antibodies. Transcription factors were stained using True-Nuclear™ Transcription Factor Buffer Set (Biolegend), according to manufacturer's protocol. For intracellular cytokine staining Cyto-Fast Fix/Perm (Biolegend) kit was used according to manufacturer's protocol. Samples were acquired on BD-LSR-II or Cytek Aurora and analyzed using FlowJo software (TreeStar Inc).

MBC transfer

Memory B cells ($B220^+IgD^-CD38^+GL7^-$) were sort-purified from *Py*-infected mice treated with rIgG or 3H3. $2x10^5$ cells were transferred intravenously to naive μMT mice, which were infected with 1×10^6 *Py* -parasitized RBCs, the following day.

Single-cell RNA sequencing analysis

Single cell suspensions were stained with Live/Dead dye (Biolegend) and then divided in a ratio of 1:4 in which 1 part was used for sorting of polyclonal cells and 4 parts were used for MSP-1 specific cells. Before staining for surface markers, MSP-1 specific cells were stained and enriched with SpyCage reagents as previously described. Both polyclonal and MSP-1 cells were incubated with fluorescently labeled antibodies and Total-seq C antibodies (Biolegend) for 30 minutes and washed before sorting for resting B cells ($B220^+IgD^+$), polyclonal ($B220^+IgD^-GL7^-CD38^+$) and MSP-1 specific ($B220^+IgD^-GL7^-CD38^+Decoy^-MSP1^+$) MBCs. Post-sorted cells were run on the 10X Chromium (10X Genomics) and library preparation was performed according to the manufacturer's protocol for Chromium Next GEM Single Cell 5' Reagent Kit v2 with Feature Barcode technology and V(D)J amplification for mouse B cells (10X Genomics). Libraries were pooled and sequenced in the Genomics and Microbiome Core Facility at Rush University using NovaSeqX Plus (Illumina). 10X Cell Ranger Multi (v.7.1.0, 10X Genomics) was used to process gene expression, CITE-seq and V(D)J libraries in each sample individually.

Downstream analysis was performed using the Seurat package[26] (version 5.1.0) with R (version 4.4.1). Samples were merged (rIgG and 3H3 groups in Polyclonal or MSP-1 specific pool) and the SCTransform[27] function using the glmGamPoi[28] package was utilized for normalization, selection of highly variable features and scaling of data. Principal component analysis (PCA) was performed and 30 dimensions were used for dimensionality reduction with Uniform Manifold Approximation and Projection (UMAP). Due to observed batch effects, the SCT datasets were integrated using the IntegrateLayers() function. Unsupervised clustering was performed using FindNeighbors() and FindClusters() function and RunUMAP() was used with reduction set to "integrated.dr". For CITE-seq, NormalizeData() and ScaleData() were used for normalization.

Differential expression analysis was performed by PrepSCTFindMarkers() followed by FindMarkers() function, which were used to identify the markers of each cluster and differentially expressed genes (DEGs) in the 3H3 compared to rIgG group. Of the identified cluster markers, only genes with adjusted p-value < 0.05 and average fold change > 0.3 were used for the heatmaps, which show the aggregated expression of all cells within a specific cluster. Of the DEGs between 3H3 versus rIgG group, only the ones with adjusted p-value < 0.05 were kept for gene ontology (GO) analysis. Enrichment for GO analysis was performed with the clusterProfiler package (v4.12.6)[29] with q- and p-value cutoffs of 0.05 and ontology set to "Biological Processes". To remove redundancy of enriched terms, the function simplify() was used. To generate a gene signature score for each cell in the SCT dataset, the function AddModuleScore() was used with gene lists of GC-derived, EF-derived or atypical MBCs (**Supp. Table 1**) . Single-cell trajectories (pseudotime analysis) were constructed using the Monocle3 package[30-34]. Cells were ordered by choosing the root cluster based on expression of genes associated with stemness and the earliest principal node was defined programmatically according to Monocle3's vignette. RColorBrewer[35], ggplot2[36], scCustomize[37] and viridis[38] packages were used for visualization of the data.

V(D)J analysis

BCR repertoire analysis was performed using Immcantation packages[39-43]. First, V, D and J genes were assigned using IgBLAST followed by removal of non-productive sequences and cells with multiple or without heavy chains. Then, cell IDs were matched with the gene expression data, cell type annotations were transferred and cells without gene expression data were removed. Clonal analysis was performed followed by generation of germline sequences. The V gene somatic hypermutation was calculated and used to compute the median mutation frequency of a clone. For visualization of data, the package ggplot2[44] was used.

Single-cell ATAC sequencing analysis

Polyclonal and MSP-1 specific MBCs were flow-sorted as described for scRNA-seq and nuclei was isolated. Transposition, barcoding on the 10X Chromium (10X Genomics) and library construction were performed according to the manufacturer's protocol for Chromium Next GEM Single Cell ATAC Reagents Kits v2 (10X Genomics). Libraries were pooled and sequenced in the Genomics and Microbiome Core Facility at Rush University using NovaSeqX Plus (Illumina). 10X Cell Ranger ATAC (v.2.1.0, 10X Genomics) was used to process the data.

Downstream analysis were performed using Seurat[26] (version 5.1.0) and Signac[45] (version 1.14.0) packages. Cells with count lower than 500 were excluded and common peak sets (for polyclonal and MSP-1 specific MBCs) were created and filtered out based on length (10000 > peak width > 20). Peaks were quantified in each sample individually and the common set of peaks was passed as the feature argument. Samples were merged (rIgG and 3H3 groups in Polyclonal or MSP-1 specific pool) as Seurat objects and features that corresponded to sequences other than the standard chromosomes were removed. After gene annotation and based on the quality control metrics, cells were filtered based on the quantified peaks (100000 > quantified peaks > 100), frequency of reads in peaks (20%), ratio of reads mapping in blacklist regions compared to peaks (0.08), nucleosome signal (signal < 4) and transcription start site enrichment (TSS > 2). Normalization, selection of top features and dimensional reduction were performed by RunTFIDF(), FindTopFeatures() and RunSVD() functions, respectively. The first LSI component was removed since it strongly correlated to sequencing depth. Clustering was performed using the FindNeighbors() function with reduction set to "lsi" followed by FindClusters() function. GeneActivity() was used to create a gene activity matrix, which was normalized and scaled by

NormalizeData() and ScaleData(), respectively. FindTransferAnchors() and TransferData() functions were used to integrate scATAC-seq data with gene expression data from the scRNA-seq. Differentially accessible regions (DARs) were calculated using the FindMarkers() function using a logistic regression (LR) model. For the total DARs, it was used a threshold of adjusted p-value < 0.05 and average log2foldchange > 0.3 and for the top DARs to be used for motif analysis it was used a threshold of adjusted p-value < 0.005 and of frequency of cells where the DAR is detected > 0.2. The list of total DARs was used to calculate the closest genes to the identified peaks, while the top DARs were used to find overrepresented motifs in the accessible regions. The list of motif position frequency matrices was obtained from JASPAR2020[46] database. was used RColorBrewer[35], scCustomize[37] and ggseqlogo[47] packages were used for visualization of the data.

Quantitative real-time PCR

MBCs were flow sorted from *Py*-infected mice that were treated with 3H3 or rIgG and then with artemether on time points indicated elsewhere. RNA was extracted using Trizol reagent according to the manufacturer's protocol. 2μg of RNA was used for cDNA synthesis using MMLV reagent. cDNA was added to the 2X PCR PowerUP SYBR Green Master mix at a 1:20 ratio, along with 0.2μM of forward and reverse primers. Primer sequences used in the experiments are as follows: *Gapdh* Fwd: 5'-GAG AAC TTT GGC ATT GTG G-3'; *Gapdh* Rev: 5'-ATG CAG GGA TGA TGT TCT G-3'; *Il9r* Fwd: 5'-GGA CAG TTG GCA GTA AGT CAC C-3'; *Il9r* Rev: 5'-CCA CTC TCT CCA AGG TCC AA-3'. *Ct* value were normalized to *Gapdh* using the following equation: $\Delta Ct = Ct\ (Il9r) - Ct(Gapdh)$. Results are represented as a ratio of *Gapdh* $2^{-(\Delta Ct)}$

Statistical analysis

Statistical analyses were performed using Prism 10 software (GraphPad). Specifics of each tests are detailed in the figure legends.

Results

Systemic 4-1BB stimulation delays effector GC response and parasite control.

In our preliminary experiments with a non-lethal rodent *Plasmodium* strain, *Plasmodium yoelii* (*Py*), we observed that 4-1BB was preferentially upregulated on splenic CD4 T cells during the course of infection (**Supp Fig. 1a**). Given the upregulation of 4-1BB, we infected (WT) C57BL/6 mice or 4-1BB$^{-/-}$ mice with *Py* and tracked the parasite load. As shown in **Supp Fig. 1b** 4-1BB$^{-/-}$ mice had an elevated parasite load compared to WT mice, suggesting a role for this receptor in anti-*Plasmodium* immune response. We next sought to investigate the effect of exogenous ligation of 4-1BB during infection. To this end, we infected WT mice with *Py* and treated them with an agonistic monoclonal antibody to 4-1BB (3H3), or the isotype control, on 5 and 7 days post-infection (dpi) (**Fig. 1a**). We then monitored the kinetics of parasite load by measuring the frequency of parasitized RBCs during the course of infection using flow cytometry as previously described[23]. As a TNFRSF member with a co-stimulatory role like OX40[48], we anticipated that 4-1BB stimulation would enhance the anti-*Plasmodium* humoral immune response. Contrary to this expectation, mice treated with 3H3 exhibited a prolonged infection course with an 8-fold higher total parasite load compared to controls, eventually resolving by 39-40 dpi (**Fig. 1b**). Additionally,

292 we observed a delayed onset of germinal center (GC) responses—both GC B cells (**Supp Fig.**
293 **1c and Fig. 1c**) and GC Tfh cells (**Supp Fig. 1d and Fig. 1d**)—in 3H3-treated mice, peaking only
294 around 39 dpi, suggesting that parasite clearance may be GC-dependent. Not surprisingly, serum
295 parasite-specific antibody levels were also slow to accumulate in 3H3-treated mice (**Fig. 1e**).
296 Confocal imaging of spleens from either group of mice revealed a pronounced disruption of
297 lymphoid architecture in 3H3-treated mice, with no apparent follicular organization until 21 dpi,
298 after which the follicles grouped into GCs as evidenced by the appearance of GL7 staining within
299 the follicles (**Fig. 1f**). Importantly, 3H3-driven loss of parasite control was reversed in mice that
300 lacked 4-1BB in CD4 T cells ($CD4^{4\text{-}1BBL\text{-}/\text{-}}$) (**Supp Fig. 1e**). These data collectively demonstrate
301 that exogenous ligation of 4-1BB on CD4 T cells in *Plasmodium*-infected mice results in derailed
302 GC responses and heightened parasite load.
303
304 **Enhanced protection following rechallenge in mice exposed to systemic 4-1BB**
305 **stimulation.**
306
307 Infection of mice with *P. berghei ANKA* (*PbA*) is invariably lethal even in mice that recovered from
308 *Py* infection. This challenge protocol is commonly used and is considered a stringent test for MBC
309 recall. Given that exogenous 4-1BB ligation delayed GC responses and increased the parasite
310 burden during the primary *Py* infection, we hypothesized that mice treated with 3H3 would exhibit
311 impaired memory responses and, consequently, reduced protection upon challenge. To test this,
312 we monitored survival in *Py*-infected mice treated with either 3H3 or rIgG after challenge with *PbA*
313 on day 90 post *Py* infection, when both groups were in convalescence (**Fig. 2a**). Surprisingly,
314 3H3-treated mice exhibited significantly longer survival compared to the rIgG group (**Fig. 2b**). To
315 directly measure MBC recall, we assessed the fold change in antibody titers between day 0 and
316 day 5 post *PbA* challenge. Consistent with the enhanced survival of 3H3-treated mice, we
317 observed a greater fold increase in anti-merozoite surface protein 1 ($MSP\text{-}1_{\text{-}19}$)-specific antibody
318 (IgM) titers between day 0 and day 5 post *PbA* challenge (**Fig. 2c**), indicating an enhanced MBC
319 recall response. An increase in parasite-specific antibody titers during this short window would
320 indicate that the antibodies are derived from PCs differentiating from an existing MBC pool, rather
321 than from a *de novo* GC reaction. The higher parasite load observed during the primary *Py*
322 infection following 3H3 treatment (**Fig. 1b**) raises the possibility that the enhanced protection
323 following *PbA* challenge may result from elevated inflammation and/or residual antigen load. To
324 investigate whether these factors influenced the outcome, we truncated the primary infection and
325 the initial parasite load by treating mice with the antimalarial drug artemether at indicated time
326 points (**Fig. 2d**). As expected, artemether treatment resulted in complete parasite clearance in
327 both groups, with 3H3 group showing no evidence of a productive GC response even by 21 dpi,
328 while rIgG group retained the GC B cell and GC Tfh cells (**Supp Fig. 2a-c**) as was seen when
329 mice were not treated with artemether (**Fig. 1**). Upon challenge with *PbA* on day 38 post-*Py*
330 infection, we observed significantly enhanced protection in 3H3-treated mice that received
331 chemoprophylaxis (**Fig. 2e**). Correspondingly, these mice also showed a higher fold change in
332 anti-MSP1 antibody titers post *PbA* challenge (**Fig. 2f**). To further test whether 3H3-mediated
333 protection is relevant to attenuated *Plasmodium* parasite vaccination, we immunized mice with
334 irradiated blood-stage *Py* parasites and administered either 3H3 or rIgG on days 5 and 7 post-
335 infection. On days 30-35 post-vaccination, the mice were challenged with *PbA* and monitored for
336 survival (**Fig. 2g**). As with live parasite infections, vaccination with irradiated parasites also
337 conferred superior protection when mice were treated with 3H3 (**Fig. 2h**), which correlated with
338 an enhanced MBC recall response, as evidenced by higher fold changes in serum antibody titers
339 (**Fig. 2i**).

In summary, these data demonstrate that systemic 4-1BB ligation, while delaying the effector GC response, significantly enhances humoral immune memory. This enhancement in memory function appears to be independent of early antigen load and holds true even when attenuated parasites are used.

Enhanced humoral immune memory stems not from larger number but higher recall potential of MBCs.

To verify whether the higher fold change in parasite-specific antibodies on day 5 post *PbA* challenge was due to larger number of antibody secreting cells (ASC), we enumerated PCs in the bone marrow of *Py*-recovered 3H3- and rIgG-treated mice challenged with *PbA.* As expected, we observed significantly larger numbers of MSP-1 specific IgM^+ PCs in 3H3-treated mice (**Fig. 3a**). As MBCs are the precursors for PCs upon antigen re-exposure[10], we determined the frequency and number of MBCs ($IgD^-CD38^+GL7^-B220^+$) prior to *PbA* challenge on 90 dpi. Contrary to our expectation, we observed significantly lower numbers of both polyclonal and antigen-specific (MSP-1 specific) (**Supp Fig. 3a, b**) MBCs in 3H3-treated mice compared to rIgG-treated ones. Upon further characterization of the MBC pool using previously described markers such as CD73, CD80 and PD-L2[49,50] to identify functionally distinct subsets**,** we observed significantly lower number of polyclonal $CD73^+CD80^+$ (**Fig. 3b**), $CD73^+PD\text{-}L2^+$ and $CD80^+PD\text{-}L2^+$ (**Supp Fig. 3c, d**) MBCs. Evaluation of MSP-1 specific MBCs also showed reduced numbers of $CD73^+PD\text{-}L2^+$, $CD80^+PD\text{-}L2^+$ (**Supp Fig. 3e, f**) pools. MSP-1 specific MBCs within the $CD73^+CD80^+$ fraction was also lower in 3H3-treated mice (**Fig. 3c**). The double positive MBC fraction has been shown to readily differentiate into ASCs while the double negative pool has been shown to reseed a secondary GC response upon antigen reencounter[12, 50]. Given that we see a rapid increase in antibody titers in just 5 days of *PbA* challenge (**Fig. 2a**), it is likely that the PCs may have readily differentiated from the existing double positive MBCs.

Given that chemoprophylaxis using artemether preserved the protective effect of 3H3 (**Fig. 2e and f**), we asked whether the PC and MBC compartments showed similar trends to what was observed without artemether. To this end, mice were infected and treated as shown in **Fig. 2d** and splenic MBCs before *PbA* challenge as well as PCs in the bone marrow 5 days post challenge were characterized. We observed lower number of polyclonal (**Fig. 3d**) as well as the MSP-1 specific (**Fig. 3e**) $CD73^+CD80^+$ MBCs in 3H3-treated mice. Despite the reduced number of MBCs and in agreement with the survival data following *PbA* challenge (**Fig. 2e**), we observed a larger frequency of PCs that stained positive for Ki67 and TACI, indicative of a high proliferative burst (**Fig. 3f**). Taken together, these data suggest that, MBCs from 3H3-treated mice are qualitatively different and are capable to differentiate and proliferate into larger number of PCs upon antigen encounter. Since artemether treatment preserves the survival advantage and cellular phenotypes, we decided to adopt this regimen as a standard approach in future experiments. This will not only allow the mice to reach convalescence early (35-40 dpi with artemether compared to 85-90 dpi without), but will also simulate the chemoprophylactic approach often used in malaria-endemic regions.

Confirming our prediction that MBCs from 3H3-treated mice may be functionally superior, they showed a higher binding affinity to MSP-1 as evidenced by a higher geometric mean fluorescence intensity of MSP-1 staining (**Fig. 3g**). To formally compare the functional capacity of these MBCs upon antigen re-exposure, we flow-sorted MBCs from 3H3- and rIgG-treated mice and adoptively transferred them into separate groups of B cell deficient (μMT) recipients that were then infected with *Py* the following day. *Py*-infected μMT mice that received MBCs from 3H3-

389 treated donors exhibited lower parasite load on 12 dpi compared to those receiving MBCs from
390 rIgG-treated donors (**Fig. 3h**) and this correlated with higher serum antibody titers (**Fig. 3i**) on 4
391 dpi. Collectively, our data so far show that MBCs derived from 3H3-treated mice exhibit
392 intrinsically superior recall potential and capacity to differentiate into antibody secreting PCs.
393
394 **Exogenous 4-1BB ligation drives extrafollicular MBCs.**
395
396 To understand the genetic basis for the functional differences between MBCs from 3H3- and rIgG-
397 treated mice, we performed scRNA-, CITE- and V(D)J- sequencing on flow-sorted polyclonal
398 ($B220^+IgD^-GL7^-CD38^+$) and MSP-1 specific ($B220^+IgD^-GL7^-CD38^+Decoy^-MSP1^+$) MBCs (**Supp**
399 **Fig. 4a**) on day 38 post *Py* infection from both groups as detailed in **Fig. 4a.** As internal controls
400 to verify our workflow, resting B cells ($B220^+IgD^+$) from either group were also spiked in to
401 represent ~ 25% of all cells sequenced in their respective polyclonal fraction. As shown in the
402 UMAP (**Supp Fig. 4b**), the polyclonal MBCs grouped into 10 different clusters with the spiked-in
403 resting B cells (IgD^+) grouping separately in cluster 1 and representing roughly 25-27% of all cells
404 sequenced (**Supp Fig. 4c**). To better highlight the potential differences among different MBC
405 populations, polyclonal cells were re-clustered without the IgD^+ population (**Fig. 4b**) into 9
406 clusters. Notably, cluster 0 was significantly more represented in the 3H3 group, comprising 55%
407 of all MBCs compared to 28% in the rIgG group (**Fig. 4c**). This cluster exhibited increased
408 expression of molecules involved with B cell activation (*Cd79a*, *Cd79b* and *Cd40*)[51-53] and survival
409 (*Tnfrsf13b* and *Tnfrsf13c*)[54-57] (**Fig. 4d**). Cluster 2 was equally represented in both groups (19-
410 20%) (**Fig 4c**) and expressed genes associated with robust activation and recall potential such
411 as *Fcrl5*[58] and *Il9r*[59], respectively (**Fig. 4d**). In contrast, clusters 1 and 3 were reduced in the 3H3
412 group relative to the rIgG group (**Fig. 4c**) and were characterized by markers associated with
413 stemness (*Sox4*, *Myb*, *Il7r* and *Cd93*)[60-63] and genes associated with GC-derived MBCs (*Plxnb2*,
414 *Basp1*, *Scimp* and *Tox*)[64], respectively (**Fig. 4d**). Intriguingly, a closer look revealed that clusters
415 0 and 2, comprising around 75% of cells derived from 3H3-treated mice (**Fig. 4c**), exhibited a
416 gene signature (**Supp table. 1**) indicative of an extrafollicular (EF) origin[64] (**Fig. 4e and f**). This is
417 consistent with our data showing a higher recall potential of MBCs from 3H3-treated mice, as EF-
418 derived MBCs have been shown to be more proliferative and result in larger number of PCs[65].
419 Finally, clusters 4-8 that showed lower EF-derived signature comprised only 6% of MBCs in the
420 3H3 group compared to nearly 22% (**Fig. 4c**) in the rIgG group and contained mostly atypical B
421 cells (**Fig. 4d, e and f**).
422 To further investigate if 3H3 treatment programs antigen-specific MBCs in a similar
423 fashion, we analyzed sequences from MSP-1 specific cells. As shown in the UMAP (**Fig. 4g**), we
424 identified 5 clusters, with cluster 0 being overrepresented in the rIgG group (67%), compared to
425 only 28% in the 3H3 group (**Fig. 4h**) and marked by high expression of genes characteristic of
426 atypical MBCs, such as *Itgax*, *Itgam*, *Itgb2* and *Fgr*[66,67] (**Fig. 4i**). Conversely, cluster 1 comprised
427 71% of MSP-1 specific MBCs in the 3H3 group, but only 20% in the rIgG group (**Fig. 4h**) and
428 characterized by a combination of markers present in clusters 0 and 2 of the polyclonal pool (**Fig.**
429 **4d and Fig. 4i**). Cluster 2 was less represented in the 3H3 group (1%) compared to the rIgG
430 group (8%) and expressed markers associated with stemness, such as *Il7r*[68,69] and *Lef1*[70] (**Fig 4h**
431 **and Fig 4i**). Clusters 3 and 4 made up less than 6% in the rIgG group and less than 0.5% in the
432 3H3 group (**Fig 4h**). Much like clusters 0 and 2 in the polyclonal pool (**Fig. 4e**), cluster 1 of the
433 MSP-1 specific pool was enriched for an EF-derived signature (**Fig 4j**), which was more
434 pronounced in 3H3-group (**Fig. 4k**), while cluster 0 (MSP-1 specific) from the rIgG group showed
435 the highest atypical signature (**Fig. 4j and k**). These data collectively demonstrate that MBCs
436 generated in mice following systemic 4-1BB stimulation is predominantly of EF origin, whereas
437 those from control mice resemble atypical MBCs.

438
439 **3H3 treatment generates MBCs with a distinct transcriptional profile supporting enhanced**
440 **recall.**
441
442 Characterization of the major clusters revealed differences in the functional composition of the
443 polyclonal and MSP-1 specific MBC pools from rIgG- and 3H3-treated mice. Importantly, cluster
444 0 in the polyclonal pool expressed the highest level of IgM (*Ighm*) (**Fig. 5a and Supp Fig. 5a**), a
445 hallmark of a highly plastic and rapidly responding MBCs following *Plasmodium* rechallenge[65];
446 while cluster 2 co-expressed CD73 (*Nt5e*), CD80 (*Cd80*) (**Fig. 5b and Supp Fig. 5b**) and
447 *Pdcd1lg2* (**Supp Fig. 5c**), markers indicative of superior recall[50]. Utilizing pseudotime inference
448 using cluster 1 as the origin, the IgM$^+$ population (cluster 0) appeared to be in the early stage of
449 its differentiation process, while clusters 2, 4 and 5 were closer to being terminally differentiated
450 (**Fig. 5c**). In contrast to MBCs from rIgG-treated mice (blue arrows, **Fig. 5c**), polyclonal MBCs
451 from 3H3-treated mice favored the early and plastic stage[65] (cluster 0, IgM$^+$) (thick red arrow, **Fig.**
452 **5c**) and had their differentiation skewed away from the terminal atypical trajectories (thin red
453 arrows, **Fig. 5c**). This will result in the preferential accumulation of IgM$^+$ EF MBCs and reduction
454 of atypical MBCs in the 3H3 group (**Fig. 4c**). Characterization of MSP-1 specific pool showed that
455 cluster 1 from 3H3-treated mice co-expressed high levels of IgM (*Ighm*) (**Fig. 5d and Supp Fig.**
456 **5d**), CD73 (*Nt5e*), CD80 (*Cd80*) (**Fig. 5e and Supp Fig. 5e**) and *Pdcd1lg2* (**Supp Fig. 5f**).
457 Pseudotime analysis using cluster 2 as the origin showed that MBCs from 3H3-treated mice
458 shifted their differentiation towards the EF trajectory (thick red arrow, **Fig. 5f**) and away from the
459 atypical trajectory (thin red arrow, **Fig. 5f**). While MBCs from the rIgG group showed a higher
460 propensity to take the atypical trajectory, away from the EF route (blue arrow, **Fig. 5f**). The data
461 so far showing that MBCs from 3H3-treated mice are more likely to have an EF origin is further
462 corroborated by our V(D)J sequencing data showing they have significantly lower mutational
463 frequency in their BCRs (**Supp Fig. 5g and h**).
464 To explore functional differences within the EF clusters, we analyzed differentially
465 expressed genes (DEGs) between rIgG and 3H3 in clusters 0 (IgM$^+$) and 2 (CD73$^+$CD80$^+$) from
466 the polyclonal pool as well as cluster 1 from the MSP-1 specific pool **(Supp. Table 2)**. Notably,
467 122 DEGs were upregulated across all 3 clusters (**Supp**. **Fig 5i**). Approximately 88% of polyclonal
468 cluster 2 DEGs were shared with polyclonal cluster 0 and/or MSP1$^+$ cluster 1, with only 21 unique
469 genes. In addition, more than half of the DEGs in polyclonal cluster 0 and MSP-1 specific cluster
470 1 were shared, underscoring the similarities between these two clusters (**Supp**. **Fig 5i**). Given
471 that most DEGs in polyclonal cluster 2 overlapped with the other 2 clusters (**Supp**. **Fig 5i**), we
472 further investigated the biological processes regulated by the combined DEGs in polyclonal
473 clusters 0 and 2 (**Fig. 5g**) and MSP-1 specific cluster 1 (**Fig. 5h**). Notably, both polyclonal and
474 MSP-1 specific MBCs from 3H3 group showed increased expression of genes associated with
475 heightened capacity for activation, proliferation and antigen presentation as well as certain
476 metabolic pathways, possibly to meet the energetic and biomass demands to support these
477 processes (**Fig 5g and Fig 5h**). In addition, MBCs from 3H3-treated mice also showed enhanced
478 cellular response to IL-4, a cytokine shown to downregulate GC related genes and enhance MBC
479 generation and activation[71,72], which may enforce the MBCs to take the extrafollicular route.
480 Aligning with these data, both the polyclonal (clusters 0 and 2, **Supp Fig. 5j**) and MSP-1 specific
481 MBCs (cluster 1, **Supp Fig. 5k**) also downregulated genes involved in pathways related to
482 increased apoptosis, reduced transcription factor binding, gene silencing and metabolism among
483 others. Collectively, these data confirm that exogenous ligation of 4-1BB results in the generation
484 of MBCs with an EF origin that are, although numerically fewer, functionally superior.
485

3H3-treatment induced protection is dependent on IFNγ and B cell intrinsic T-BET:IL-9R axis.

Previous studies have highlighted the role of B cell intrinsic IFNγ signaling and T-BET expression [73-75] for enhanced MBC recall and PC differentiation. Importantly, exogenous stimulation of 4-1BB was shown to result in higher levels of IFNγ secretion by CD4 T cells[76]. When splenocytes were stimulated in the presence of PMA/Ionomycin and brefeldin A, we observed that CD4 T cells derived from 3H3-treated mice were indeed capable of secreting higher levels of IFNγ (**Supp Fig 6a**). Additionally, B cells cultured *ex vivo* with IFNγ showed a significant increase in T-BET expression within 18 hours (**Supp Fig. 6b**). In line with this, we also observed significantly higher expression of T-BET in activated (IgD^-) B cells derived from 3H3-treated mice around 15 dpi (**Supp Fig. 6c**). T-BET expression in B cells during the effector phase was shown to enhance protection from rechallenge by mediating class-switching to IgG2c antibody isotype[73]. Consistent with this finding, we observed higher increases in IgG2c levels following *PbA* challenge in 3H3-treated mice (**Supp Fig. 6d**). Given these data, we asked whether 3H3-mediated superior protection is IFNγ dependent. To test this, mice were infected with *Py* and treated with 3H3 or rIgG and IFNγ was blocked using IFNγ blocking antibody (XMG1.2) on indicated timepoints. Mice were then challenged with *PbA* (around 90 dpi) and survival was monitored (**Supp Fig. 6e**). As expected, 3H3-treated mice lost protection following *PbA* challenge when IFNγ was blocked (**Supp Fig. 6f**). Given the link between IFNγ and T-BET, we then asked whether B cell intrinsic T-BET expression is necessary for 3H3-mediated protection. To this end, we generated mixed bone marrow chimeras in which T-BET deficiency was restricted to the B cell compartment ($B^{Tbx21-/-}$) (**Supp Fig. 6g**) and infected them with *Py,* followed by 3H3 treatment. Similar to our results from XMG1.2 treatment, *PbA* challenge of convalescent $B^{Tbx21-/-}$ mice showed significantly reduced survival compared to B^{WT} mice (**Supp Fig. 6h**). Taken together, these highlight the importance of IFNγ:T-BET axis during *Plasmodium* infection and show that the enhanced protection observed in mice subjected to exogenous 4-1BB ligation is dependent on this axis.

IL-9 receptor (IL-9R) signaling on MBCs has also been shown to result in superior recall[59]. In line with this, MSP-1 specific MBCs from 3H3-treated mice subjected to IFNγ blockade and $B^{Tbx21-/-}$ mice showed significantly lower levels of IL-9R expression (**Supp Fig. 6i and j**) suggesting that B cell intrinsic IFNγ:T-BET axis is key to this phenomenon. To investigate the contribution of IL-9R to higher MBC recall, we searched for distinct *Il9r*-expressing cluster(s) in our scRNA-seq data and identified polyclonal (cluster 2) (**Fig. 6a**) and MSP-1 specific (cluster 1) (**Fig. 6b**) which also co-expressed other signature MBC markers such *as Nt5e, Cd80, Pdcd1lg2* among others (**Fig. 4d**). Quantitative real-time PCR analysis on flow-sorted MBCs from 3H3-treated mice also showed significantly higher levels of *Il9r* expression compared to those from rIgG-treated mice (**Supp. Fig 7a**). In an attempt to draw parallels among populations from our transcriptomic and flow cytometry datasets, we clustered our multi-parameter flow cytometry data in a UMAP space (polyclonal, **Fig. 6c** and MSP-1 specific, **Fig. 6f**). As shown in **Fig. 6c** and **d,** the polyclonal pool clustered into 9 populations (*A-I*), of which populations *D* and *I* denoted the MSP-1 specific pool. While populations *E, F* and *I* expressed IL-9R, population E failed to express key functional markers such as CD73 and CD80 making it less likely to be involved in an immediate recall following antigen re-exposure (**Fig. 6d** and **Supp Fig. 7b**). Importantly and in agreement with this, we observed that the $CD73^+CD80^+$ MBC population from 3H3-treated mice expressed significantly higher levels of IL-9R compared to controls (**Fig. 6e**). These data also suggested that population *I* may be functionally similar to population *F* and together they may represent antigen-specific MBC pools that are swiftly recalled following antigen-reencounter. Phenotypic dissimilarity of populations *D* and *I* also highlights the functional heterogeneity within a given

534 antigen-specific pool. This was confirmed by further clustering the MSP-1 specific pool which
535 yielded 5 different populations, mostly differing in their expression of key functional MBC markers
536 (**Fig. 6f and g**). As with the polyclonal cells (**Fig.6e**), MSP-1 specific MBCs from 3H3-treated mice
537 also expressed higher levels of IL-9R (**Fig. 6h**) suggestive of their superior recall potential. Given
538 the parallels between the gene and surface maker expression data, polyclonal cluster 2 may be
539 identical to population *F* and they may represent MBCs equipped to readily engage in a recall
540 response. Given the dependency on IFNγ and B cell intrinsic T-BET expression for heightened
541 survival of 3H3-treated mice, we hypothesized that IL-9R expression may also be regulated by
542 this axis. To test this, B cells from naïve mice were activated *ex vivo* in the presence or absence
543 of IFNγ and IL-9R expression was evaluated after 3 days in culture. Although activation of B cells
544 alone resulted in increase in IL-9R expression, it was further increased when IFNγ was added
545 to the culture (**Supp Fig. 7c**).
546 To investigate whether the enhanced protection following *PbA* challenge in 3H3-treated
547 mice is dependent on IL-9:IL-9R signaling, we blocked IL-9 in convalescent mice prior to *PbA*
548 challenge and monitored survival (**Supp Fig. 7d)**. As shown in **Fig**. **6i**, the enhanced protection
549 observed in 3H3-treated mice was reversed in mice treated with IL-9 blocking antibody compared
550 to controls; rIgG-treated mice did not show any difference in survival. Supporting our observation,
551 3H3-treated mice subjected to IL-9 neutralization exhibited a blunted antibody recall following *PbA*
552 challenge (**Fig. 6j**), indicating that IL-9 signaling is important for 3H3-mediated protection. Next,
553 we interrogated whether B cell-intrinsic IL-9R expression is important for the enhanced protection
554 following 3H3 treatment. To accomplish this, we generated competitive mixed bone marrow
555 chimeras in which IL-9R deficiency is restricted to B cells ($B^{Il9r-/-}$) (**Supp Fig. 7e**). Since we did not
556 see any difference in the rIgG treated mice following IL-9 blockade (**Fig. 6i**), we confined our
557 experiment to 3H3-treatment in $B^{Il9r-/-}$ and B^{WT} mice. On 38 dpi, mice were challenged with *PbA*
558 and survival was monitored. Notably, we observed that $B^{Il9r-/-}$ mice showed significantly shorter
559 survival than B^{WT} mice following *PbA* challenge (**Fig. 6k**) and a dampened MBC recall response
560 as evident from the lower fold change in serum antibody titers (**Fig. 6l**). These data show that the
561 MBC recall following *PbA* challenge in 3H3-treated mice is dependent on the B cell-intrinsic IL-
562 9R expression. Collectively, our data highlight a previously underappreciated IFNγ:T-BET:IL-9R
563 axis present in MBCs following *Plasmodium* infection, which could potentially be modulated to
564 enhance humoral immune memory.
565
566 **Exogenous 4-1BB ligation poises MBCs for swift recall by altering their epigenome.**
567
568 Given that both polyclonal and MSP-1 specific MBCs from 3H3-treated mice downregulated
569 genes associated with transcriptional silencing and regulation of transcription factor activity
570 (**Supp. Fig 5j and k**), we wanted to determine whether these MBCs are imprinted with an
571 epigenetic signature supporting superior recall. To this end, we flow-sorted polyclonal and MSP-
572 1 specific MBCs from 3H3- or rIgG-treated mice (**Fig. 7a**) as before and performed scATAC-seq.
573 Initial clustering based on transposase activity populated 4 different clusters in the MSP-1 specific
574 cells (**Supp. Fig 8a**) and 6 clusters in the polyclonal pool (**Supp. Fig 8b**). Given the importance
575 of B cell-intrinsic IL-9R expression in mice treated with 3H3, we wanted to identify the IL-9R
576 expressing population in our scATAC-seq dataset and examine the accessibility of genes that can
577 potentiate PC differentiation. Thus, we integrated our scRNA-seq (from **Fig. 4 and 5**) with the
578 scATAC-seq datasets and used the transferred labels to annotate the ATAC clusters from MSP1-
579 specific (**Fig. 7b**) and polyclonal MBCs (**Supp Fig. 8c**). As shown in **Fig. 7b**, following integration,
580 most cells fell in either cluster 0 or 1. Since cluster 1 in MSP-1 specific MBCs expressed the
581 highest level of *Il9r* (**Fig. 6b**), we examined whether the *Il9r* gene locus in this cluster is still

accessible. As shown in **Fig. 7c**, we observed significantly higher accessibility in the *Il9r* locus in cluster 1 compared to cluster 0, showing that MBCs in cluster 1 are imprinted with an epigenome that favors higher *Il9r* expression. In line with our prediction that IL-9R expressing MBCs are primed to quickly differentiate into PCs, cluster 1 also showed enhanced accessibility for *Prdm1* locus (**Fig. 7d**) as well as for key transcription factors (TF) binding motifs (XBP1, ATF3, MYC, ATF6, KLF6 and BHLHE40) (**Fig. 7e**) associated with enhanced PC differentiation. Importantly and similar to cluster 1 in the MSP-1 specific pool, cluster 2 in the polyclonal pool also showed significantly enhanced *Il9r* locus accessibility (**Supp Fig. 8d**) as well as markers of higher activation potential (*Fclr5*, **Supp Fig. 8e**), enhanced PC differentiation (*Atf6*, **Supp. Fig 8f**) and antiapoptotic signaling (*Bcl2*, **Supp Fig. 8g**). In addition, TF binding motifs important in PC differentiation (KLF4, ATF3, XBP1 and IRF4) as well as cell proliferation (MYC) and IFNγ signaling (IRF1) were also accessible in cluster 2 from the polyclonal pool (**Supp Fig.8h**). Given that *Il9r* expression correlates with enhanced protection in 3H3-treated mice, we compared the chromatin accessibility of *Il9r*-expressing MBCs between 3H3- and rIgG-treated groups. In strong agreement with our survival and phenotypic data, MBCs from 3H3-treated mice in cluster 1 not only showed continued accessibility for *Il9r* locus (**Fig. 7f**), but were also enriched for the key transcription factor binding motifs associated with enhanced PC differentiation and proliferation (**Fig. 7g**). Notably, we also observed that T-BET and IRF1 binding motifs also showed higher accessibility further reinforcing our finding that the superior recall we observe in 3H3-treated mice is dependent on IFNγ:T-BET:IL-9R axis.

Discussion

In this study, we investigated the effects of exogenous 4-1BB ligation and observed an unexpected outcome in MBC generation in an experimental mouse model of malaria. Despite the disruption of the effector GC response and a total reduction in MBC numbers, the MBC recall response was significantly enhanced, providing protection upon reinfection. While our data draw some parallels with a previous study using a viral infection model [77] showing a derailed GC response, our findings on humoral immune memory response are unique. Single-cell transcriptomic analysis of the MBCs showed a predominant extrafollicular rather than a GC-derived signature, with IL-9R emerging as a key determinant for the enhanced recall. Using a combination of genetic, chimeric, and biochemical approaches, we identify a previously unappreciated axis comprising IFNγ and B cell intrinsic T-BET expression during the effector phase, potentially driving the expression of IL-9R. Sequencing for transposase-accessible chromatin regions in flow-sorted MBCs from *Plasmodium*-infected mice treated with exogenous 4-1BB agonist also revealed an epigenomic landscape that primed them for rapid differentiation into PCs.

Similar to our study, *Ehrlichia muris (E. muris)* infection alone without the need of any agonistic antibody to 4-1BB, resulted in a derailed GC response[78]. Notably, the MBCs that appeared in *E. muris* infection were $CD11c^+$ and T-dependent but seldom expressed GC-related markers[79]. Thus, the antigen-specific IgM^+ MBCs (cluster 1) in our study are largely similar to MBCs mentioned in the study above[79], but express FCLR5 and not CD11c. Co-expression of CD11c, CD11b and FCLR5 are considered markers for atypical MBCs, with predominantly inhibitory functions [80-82]. Based on the lack of CD11b and CD11c expression combined with the expression of various activation markers (**Fig. 4 and 6**) including FCLR5[58], we contend that the IgM^+ MBCs from 3H3-treated mice (cluster 1) are different from the inhibitory atypical MBCs.

IFNγ-driven T-BET expression was shown to be pivotal to increased protection following *Plasmodium* rechallenge[73]. Reliance on IFNγ:T-BET axis in 3H3-treated mice for enhanced recall, along with a pronounced EF signature of these MBCs, is in agreement with previous findings

631 showing that B cell-intrinsic IFNγ signaling reinforces EF B cell responses[83]. Previous studies
632 have also independently shown the role of IL-9R expression for enhanced recall[59]. 3H3-treated
633 but not rIgG-treated mice, seem to depend on IL-9R expression specifically on B cells for
634 protection, which may be explained by the far lower IL-9R expression in MBCs derived from rIgG-
635 treated mice. Our scATAC-seq data shows that IRF1 binding motifs are readily accessible in *Il9r*
636 expressing MBCs from both groups showing responsiveness to IFNγ[84]. More importantly, MBCs
637 from 3H3-treated mice have a more pronounced accessibility to this region along with T-BET
638 binding motifs. This further strengthens the possibility that IFNγ-driven T-BET may influence the
639 expression of IL-9R in MBCs from 3H3-treated mice. We also observed lower IL-9R levels in B
640 cells lacking T-BET expression or when IFNγ was blocked, which is complemented by our finding
641 that IL-9R expression can be enhanced in B cells when subjected to IFNγ *ex vivo*. Together, these
642 data suggest a potential role of IFNγ:T-BET axis in IL-9R expression and raises the possibility that
643 T-BET levels may have to reach a specific threshold to enforce IL-9R expression. While these
644 observations are B cell-centric, the source of IL-9 during the memory phase to signal via IL-9R
645 remains to be investigated. As such, stimulation of various TNFRSF members have been shown
646 to promote IL-9 secretion from CD4 T cells in multiple experimental settings[85,86-88]. Although our
647 IL-9 neutralization experiments suggest the presence of an IL-9 source prevalent during the
648 memory phase, a direct determination of the identity of the cellular source is yet to be done. IL-9
649 neutralization during the memory phase compromised survival and MBC recall only in 3H3-treated
650 mice, signifying the role of IL-9:IL-9R signaling following 4-1BB stimulation. To our knowledge,
651 our study remains the first of its kind to link the IFNγ:T-BET axis with IL-9R in MBC recall. Despite
652 mining numerous publicly available human malaria datasets studying MBCs, we were unable to
653 find a high IL-9R expressing population that could be correlated with enhanced protection upon
654 pathogen re-exposure. This is due to the fact that none of these studies involved the use of
655 immunomodulatory approaches that potentially drive high T-BET in B cells, which may be key to
656 driving IL-9R. Indeed, our own *ex vivo* data with murine B cells stimulated with IFNγ resulted in
657 the upregulation of T-BET first and IL-9R later (T-BET expression preceding IL-9R). A fate
658 mapping approach capable of tracking T-BET expression would be the ideal strategy to directly
659 ask this question, but it remains beyond the scope of this manuscript.
660 Although many studies have focused on the effect of 4-1BB on CD8 T cells[89,90], systemic
661 ligation of 4-1BB has been shown to reprogram CD4 T cells in a virus infection setting as well[76].
662 It is unlikely that 4-1BB stimulation on CD8 T cells may play a significant role in our studies, as
663 CD8 T cell depletion in 3H3-treated mice still disrupted the effector germinal center (GC) response
664 and resulted in substantial loss of parasite control, similar to observed in CD8 T cell replete WT
665 mice (*Caloba and Vijay unpublished data*). B cells are also known to express 4-1BB[91], but we did
666 not explore the role of 4-1BB stimulation on B cells as CD4-specific 4-1BB$^{-/-}$ bone marrow
667 chimeras failed to respond to 3H3 treatment as it did not derail the parasite control. These findings
668 indicate that in rodent malaria models, the effects of exogenous 4-1BB stimulation are dependent
669 on CD4 T cell intrinsic 4-1BB expression.
670 Here we provide data showing that exogenous 4-1BB stimulation is capable of programing
671 a predominantly EF B cell response that generates antigen-specific MBCs with superior recall
672 potential. Importantly, although the MBCs in mice that received 4-1BB stimulation is at a numerical
673 disadvantage, a large fraction of those cells possess a distinct epigenetic landscape and
674 transcriptional signature poising them for swift and efficient recall. Single-cell trajectory analysis
675 also reveals that MBCs from 3H3-treated mice have a tendency to stay more plastic within the
676 extrafollicular space. Our data also brings up the argument that GC response during effector
677 phase cannot always be a predictor for the ensuing memory response. We show that 4-1BB is a
678 compelling target for host-directed immunotherapy in infections that are reliant on MBC-driven
679 antibody response for protection. While the widescale use of a monoclonal antibody as an

immunotherapy may be cost prohibitive, the prospect of synthesizing small molecule activators of 4-1BB for achieving potent humoral memory immune activation and thus durable and long-lasting protection may be practical.

Acknowledgements

The authors thank all past and present members of the Vijay Lab for the helpful dicussions and technical assistance. We thank Drs. Fabio Re (RFUMS) and Danielle Stanisic (Griffith University) for the critical review of the manuscript. We thank the RFUMS flow cytometry facility for the instrumentation as well as the Biological Research Facility for animal husbandry and maintenance. We thank Dr. Stefan Green, Kevin Kunstman, Edith Perez and Ping Li at the Genomics and Microbiome Core Facility at Rush University for help with sequencing. This work was supported by the RFUMS startup funds and Schweppe Scholar Award to R.V and the AAI 2024 Careers in Immunology Fellowship to C.C. and R.V.

Author Contributions

R.V. conceived the study. C.C. and R.V. designed, executed, analyzed and wrote the manuscript. C.C. also performed the bioinformatic data analyses. A.J.S. executed experiments. T.A.L., L.J., and A.R., provided technical assistance. A.M.M and S.E.L. generated and provided reagents, T.H.W. provided reagents as well as provided intellectual input, A.M.C. and M.H.K. generated and provided reagents, M.H.K. provided intellectual input, J.P.W. provided technical assistance for bioinformatic analyses.

704 References
705
706 1. WHO World malaria report 2023. Geneva: World Health Organization;2023.
707 2. Cowman, A.F., Healer, J., Marapana, D., and Marsh, K. (2016). Malaria: Biology and
708 Disease. Cell *167*, 610-624. 10.1016/j.cell.2016.07.055.
709 3. Laurens, M.B. (2020). RTS,S/AS01 vaccine (Mosquirix): an overview. Hum Vaccin
710 Immunother *16*, 480-489. 10.1080/21645515.2019.1669415.
711 4. MacLennan, I.C. (1994). Germinal centers. Annual review of immunology *12*, 117-139.
712 10.1146/annurev.iy.12.040194.001001.
713 5. Cohen, S., Mc, G.I., and Carrington, S. (1961). Gamma-globulin and acquired immunity
714 to human malaria. Nature *192*, 733-737. 10.1038/192733a0.
715 6. Liu, Y.J., Malisan, F., de Bouteiller, O., Guret, C., Lebecque, S., Banchereau, J., Mills,
716 F.C., Max, E.E., and Martinez-Valdez, H. (1996). Within germinal centers, isotype switching of
717 immunoglobulin genes occurs after the onset of somatic mutation. Immunity *4*, 241-250.
718 10.1016/s1074-7613(00)80432-x.
719 7. Jacob, J., Kelsoe, G., Rajewsky, K., and Weiss, U. (1991). Intraclonal generation of
720 antibody mutants in germinal centres. Nature *354*, 389-392. 10.1038/354389a0.
721 8. Berek, C., Berger, A., and Apel, M. (1991). Maturation of the immune response in
722 germinal centers. Cell *67*, 1121-1129. 10.1016/0092-8674(91)90289-b.
723 9. Nutt, S.L., Hodgkin, P.D., Tarlinton, D.M., and Corcoran, L.M. (2015). The generation of
724 antibody-secreting plasma cells. Nat Rev Immunol *15*, 160-171. 10.1038/nri3795.
725 10. Inoue, T., and Kurosaki, T. (2024). Memory B cells. Nat Rev Immunol *24*, 5-17.
726 10.1038/s41577-023-00897-3.
727 11. Good-Jacobson, K.L., and Shlomchik, M.J. (2010). Plasticity and heterogeneity in the
728 generation of memory B cells and long-lived plasma cells: the influence of germinal center
729 interactions and dynamics. Journal of immunology *185*, 3117-3125. 10.4049/jimmunol.1001155.
730 12. Kurosaki, T., Kometani, K., and Ise, W. (2015). Memory B cells. Nat Rev Immunol *15*,
731 149-159. 10.1038/nri3802.
732 13. Tran, T.M., Li, S., Doumbo, S., Doumtabe, D., Huang, C.Y., Dia, S., Bathily, A., Sangala,
733 J., Kone, Y., Traore, A., et al. (2013). An intensive longitudinal cohort study of Malian children
734 and adults reveals no evidence of acquired immunity to Plasmodium falciparum infection. Clin
735 Infect Dis *57*, 40-47. 10.1093/cid/cit174.
736 14. Butler, N.S., Moebius, J., Pewe, L.L., Traore, B., Doumbo, O.K., Tygrett, L.T.,
737 Waldschmidt, T.J., Crompton, P.D., and Harty, J.T. (2011). Therapeutic blockade of PD-L1 and
738 LAG-3 rapidly clears established blood-stage Plasmodium infection. Nat Immunol *13*, 188-195.
739 10.1038/ni.2180.
740 15. Kurup, S.P., Obeng-Adjei, N., Anthony, S.M., Traore, B., Doumbo, O.K., Butler, N.S.,
741 Crompton, P.D., and Harty, J.T. (2017). Regulatory T cells impede acute and long-term
742 immunity to blood-stage malaria through CTLA-4. Nat Med *23*, 1220-1225. 10.1038/nm.4395.
743 16. Zander, R.A., Obeng-Adjei, N., Guthmiller, J.J., Kulu, D.I., Li, J., Ongoiba, A., Traore, B.,
744 Crompton, P.D., and Butler, N.S. (2015). PD-1 Co-inhibitory and OX40 Co-stimulatory Crosstalk
745 Regulates Helper T Cell Differentiation and Anti-Plasmodium Humoral Immunity. Cell Host
746 Microbe *17*, 628-641. 10.1016/j.chom.2015.03.007.
747 17. Zander, R.A., Vijay, R., Pack, A.D., Guthmiller, J.J., Graham, A.C., Lindner, S.E.,
748 Vaughan, A.M., Kappe, S.H.I., and Butler, N.S. (2017). Th1-like Plasmodium-Specific Memory
749 CD4(+) T Cells Support Humoral Immunity. Cell Rep *21*, 1839-1852.
750 10.1016/j.celrep.2017.10.077.
751 18. Illingworth, J., Butler, N.S., Roetynck, S., Mwacharo, J., Pierce, S.K., Bejon, P.,
752 Crompton, P.D., Marsh, K., and Ndungu, F.M. (2013). Chronic exposure to Plasmodium

753 falciparum is associated with phenotypic evidence of B and T cell exhaustion. Journal of
754 immunology *190*, 1038-1047. 10.4049/jimmunol.1202438.
755 19. Dawicki, W., Bertram, E.M., Sharpe, A.H., and Watts, T.H. (2004). 4-1BB and OX40 act
756 independently to facilitate robust CD8 and CD4 recall responses. Journal of immunology *173*,
757 5944-5951. 10.4049/jimmunol.173.10.5944.
758 20. Dawicki, W., and Watts, T.H. (2004). Expression and function of 4-1BB during CD4
759 versus CD8 T cell responses in vivo. Eur J Immunol *34*, 743-751. 10.1002/eji.200324278.
760 21. Kwon, B.S., Hurtado, J.C., Lee, Z.H., Kwack, K.B., Seo, S.K., Choi, B.K., Koller, B.H.,
761 Wolisi, G., Broxmeyer, H.E., and Vinay, D.S. (2002). Immune responses in 4-1BB (CD137)-
762 deficient mice. Journal of immunology *168*, 5483-5490. 10.4049/jimmunol.168.11.5483.
763 22. Vijay, R., Guthmiller, J.J., Sturtz, A.J., Surette, F.A., Rogers, K.J., Sompallae, R.R., Li,
764 F., Pope, R.L., Chan, J.A., de Labastida Rivera, F., et al. (2020). Infection-induced plasmablasts
765 are a nutrient sink that impairs humoral immunity to malaria. Nat Immunol *21*, 790-801.
766 10.1038/s41590-020-0678-5.
767 23. Malleret, B., Claser, C., Ong, A.S., Suwanarusk, R., Sriprawat, K., Howland, S.W.,
768 Russell, B., Nosten, F., and Renia, L. (2011). A rapid and robust tri-color flow cytometry assay
769 for monitoring malaria parasite development. Sci Rep *1*, 118. 10.1038/srep00118.
770 24. Villarino, N.F., LeCleir, G.R., Denny, J.E., Dearth, S.P., Harding, C.L., Sloan, S.S.,
771 Gribble, J.L., Campagna, S.R., Wilhelm, S.W., and Schmidt, N.W. (2016). Composition of the
772 gut microbiota modulates the severity of malaria. Proc Natl Acad Sci U S A *113*, 2235-2240.
773 10.1073/pnas.1504887113.
774 25. Johnson, J.T., Surette, F.A., Ausdal, G.R., Shah, M., Minns, A.M., Lindner, S.E., Zander,
775 R.A., and Butler, N.S. (2024). CD4 T Cell-Derived IL-21 Is Critical for Sustaining Plasmodium
776 Infection-Induced Germinal Center Responses and Promoting the Selection of Memory B Cells
777 with Recall Potential. Journal of immunology *212*, 1467-1478. 10.4049/jimmunol.2300683.
778 26. Butler, A., Hoffman, P., Smibert, P., Papalexi, E., and Satija, R. (2018). Integrating
779 single-cell transcriptomic data across different conditions, technologies, and species. Nat
780 Biotechnol *36*, 411-420. 10.1038/nbt.4096.
781 27. Choudhary, S., and Satija, R. (2022). Comparison and evaluation of statistical error
782 models for scRNA-seq. Genome Biol *23*, 27. 10.1186/s13059-021-02584-9.
783 28. Ahlmann-Eltze, C., and Huber, W. (2021). glmGamPoi: fitting Gamma-Poisson
784 generalized linear models on single cell count data. Bioinformatics *36*, 5701-5702.
785 10.1093/bioinformatics/btaa1009.
786 29. Xu, S., Hu, E., Cai, Y., Xie, Z., Luo, X., Zhan, L., Tang, W., Wang, Q., Liu, B., Wang, R.,
787 et al. (2024). Using clusterProfiler to characterize multiomics data. Nature protocols *19*, 3292-
788 3320. 10.1038/s41596-024-01020-z.
789 30. Trapnell, C., Cacchiarelli, D., Grimsby, J., Pokharel, P., Li, S., Morse, M., Lennon, N.J.,
790 Livak, K.J., Mikkelsen, T.S., and Rinn, J.L. (2014). The dynamics and regulators of cell fate
791 decisions are revealed by pseudotemporal ordering of single cells. Nat Biotechnol *32*, 381-386.
792 10.1038/nbt.2859.
793 31. Qiu, X., Mao, Q., Tang, Y., Wang, L., Chawla, R., Pliner, H.A., and Trapnell, C. (2017).
794 Reversed graph embedding resolves complex single-cell trajectories. Nat Methods *14*, 979-982.
795 10.1038/nmeth.4402.
796 32. Cao, J., Spielmann, M., Qiu, X., Huang, X., Ibrahim, D.M., Hill, A.J., Zhang, F., Mundlos,
797 S., Christiansen, L., Steemers, F.J., et al. (2019). The single-cell transcriptional landscape of
798 mammalian organogenesis. Nature *566*, 496-502. 10.1038/s41586-019-0969-x.
799 33. Traag, V.A., Waltman, L., and van Eck, N.J. (2019). From Louvain to Leiden:
800 guaranteeing well-connected communities. Sci Rep *9*, 5233. 10.1038/s41598-019-41695-z.

801 34. Levine, J.H., Simonds, E.F., Bendall, S.C., Davis, K.L., Amir el, A.D., Tadmor, M.D.,
802 Litvin, O., Fienberg, H.G., Jager, A., Zunder, E.R., et al. (2015). Data-Driven Phenotypic
803 Dissection of AML Reveals Progenitor-like Cells that Correlate with Prognosis. Cell *162*, 184-
804 197. 10.1016/j.cell.2015.05.047.
805 35. Neuwirth, E. (2022). RColorBrewer: ColorBrewer Palettes.
806 36. Planche, T., Dzeing, A., Emmerson, A.C., Onanga, M., Kremsner, P.G., Engel, K.,
807 Kombila, M., Ngou-Milama, E., and Krishna, S. (2002). Plasma glutamine and glutamate
808 concentrations in Gabonese children with Plasmodium falciparum infection. QJM *95*, 89-97.
809 10.1093/qjmed/95.2.89.
810 37. Marsh, S. (2021). scCustomize: Custom Visualizations & Functions for Streamlined
811 Analyses of Single Cell Sequencing.
812 38. Garnier, S., Ross, Noam, Rudis, Robert, Camargo, Pedro A, Sciaini, Marco, Scherer,
813 Cédric (2024). Colorblind-Friendly Color Maps for R. 10.5281/zenodo.4679423.
814 39. Gupta, N.T., Vander Heiden, J.A., Uduman, M., Gadala-Maria, D., Yaari, G., and
815 Kleinstein, S.H. (2015). Change-O: a toolkit for analyzing large-scale B cell immunoglobulin
816 repertoire sequencing data. Bioinformatics *31*, 3356-3358. 10.1093/bioinformatics/btv359.
817 40. Nouri, N., and Kleinstein, S.H. (2018). A spectral clustering-based method for identifying
818 clones from high-throughput B cell repertoire sequencing data. Bioinformatics *34*, i341-i349.
819 10.1093/bioinformatics/bty235.
820 41. Nouri, N., and Kleinstein, S.H. (2020). Somatic hypermutation analysis for improved
821 identification of B cell clonal families from next-generation sequencing data. PLoS Comput Biol
822 *16*, e1007977. 10.1371/journal.pcbi.1007977.
823 42. Gupta, N.T., Adams, K.D., Briggs, A.W., Timberlake, S.C., Vigneault, F., and Kleinstein,
824 S.H. (2017). Hierarchical Clustering Can Identify B Cell Clones with High Confidence in Ig
825 Repertoire Sequencing Data. Journal of immunology *198*, 2489-2499.
826 10.4049/jimmunol.1601850.
827 43. Hoehn, K.B., Pybus, O.G., and Kleinstein, S.H. (2022). Phylogenetic analysis of
828 migration, differentiation, and class switching in B cells. PLoS Comput Biol *18*, e1009885.
829 10.1371/journal.pcbi.1009885.
830 44. Wickham, H. (2016). ggplot2: Elegant Graphics for Data Analysis. Springer-Verlag New
831 York.
832 45. Stuart, T., Srivastava, A., Madad, S., Lareau, C.A., and Satija, R. (2021). Single-cell
833 chromatin state analysis with Signac. Nat Methods *18*, 1333-1341. 10.1038/s41592-021-01282-
834 5.
835 46. Fornes, O., Castro-Mondragon, J.A., Khan, A., van der Lee, R., Zhang, X., Richmond,
836 P.A., Modi, B.P., Correard, S., Gheorghe, M., Baranasic, D., et al. (2020). JASPAR 2020:
837 update of the open-access database of transcription factor binding profiles. Nucleic Acids Res
838 *48*, D87-D92. 10.1093/nar/gkz1001.
839 47. Wagih, O. (2024). ggseqlogo: A 'ggplot2' Extension for Drawing Publication-Ready
840 Sequence Logos. https://CRAN.R-project.org/package=ggseqlogo.
841 48. Arch, R.H., and Thompson, C.B. (1998). 4-1BB and Ox40 are members of a tumor
842 necrosis factor (TNF)-nerve growth factor receptor subfamily that bind TNF receptor-associated
843 factors and activate nuclear factor kappaB. Mol Cell Biol *18*, 558-565. 10.1128/MCB.18.1.558.
844 49. Brown, S.L., Bauer, J.J., Lee, J., Ntirandekura, E., and Stumhofer, J.S. (2022). IgM(+)
845 and IgM(-) memory B cells represent heterogeneous populations capable of producing class-
846 switched antibodies and germinal center B cells upon rechallenge with P. yoelii. Journal of
847 leukocyte biology *112*, 1115-1135. 10.1002/JLB.4A0921-523R.
848 50. Zuccarino-Catania, G.V., Sadanand, S., Weisel, F.J., Tomayko, M.M., Meng, H.,
849 Kleinstein, S.H., Good-Jacobson, K.L., and Shlomchik, M.J. (2014). CD80 and PD-L2 define

850 functionally distinct memory B cell subsets that are independent of antibody isotype. Nat
851 Immunol *15*, 631-637. 10.1038/ni.2914.
852 51. Huse, K., Bai, B., Hilden, V.I., Bollum, L.K., Vatsveen, T.K., Munthe, L.A., Smeland,
853 E.B., Irish, J.M., Walchli, S., and Myklebust, J.H. (2022). Mechanism of CD79A and CD79B
854 Support for IgM+ B Cell Fitness through B Cell Receptor Surface Expression. Journal of
855 immunology *209*, 2042-2053. 10.4049/jimmunol.2200144.
856 52. Tkachenko, A., Kupcova, K., and Havranek, O. (2023). B-Cell Receptor Signaling and
857 Beyond: The Role of Igalpha (CD79a)/Igbeta (CD79b) in Normal and Malignant B Cells. Int J
858 Mol Sci *25*. 10.3390/ijms25010010.
859 53. Carpenter, E.L., Mick, R., Ruter, J., and Vonderheide, R.H. (2009). Activation of human
860 B cells by the agonist CD40 antibody CP-870,893 and augmentation with simultaneous toll-like
861 receptor 9 stimulation. J Transl Med *7*, 93. 10.1186/1479-5876-7-93.
862 54. Luo, W., Weisel, F., and Shlomchik, M.J. (2018). B Cell Receptor and CD40 Signaling
863 Are Rewired for Synergistic Induction of the c-Myc Transcription Factor in Germinal Center B
864 Cells. Immunity *48*, 313-326 e315. 10.1016/j.immuni.2018.01.008.
865 55. He, B., Santamaria, R., Xu, W., Cols, M., Chen, K., Puga, I., Shan, M., Xiong, H.,
866 Bussel, J.B., Chiu, A., et al. (2010). The transmembrane activator TACI triggers immunoglobulin
867 class switching by activating B cells through the adaptor MyD88. Nat Immunol *11*, 836-845.
868 10.1038/ni.1914.
869 56. Eslami, M., Schuepbach-Mallepell, S., Diana, D., Willen, L., Kowalczyk-Quintas, C.,
870 Desponds, C., Peter, B., Vigolo, M., Renevey, F., Donze, O., et al. (2024). Unique and
871 redundant roles of mouse BCMA, TACI, BAFF, APRIL, and IL-6 in supporting antibody-
872 producing cells in different tissues. Proc Natl Acad Sci U S A *121*, e2404309121.
873 10.1073/pnas.2404309121.
874 57. Lau, A.W.Y., Turner, V.M., Bourne, K., Hermes, J.R., Chan, T.D., and Brink, R. (2021).
875 BAFFR controls early memory B cell responses but is dispensable for germinal center function.
876 The Journal of experimental medicine *218*. 10.1084/jem.20191167.
877 58. Kim, C.C., Baccarella, A.M., Bayat, A., Pepper, M., and Fontana, M.F. (2019). FCRL5(+)
878 Memory B Cells Exhibit Robust Recall Responses. Cell Rep *27*, 1446-1460 e1444.
879 10.1016/j.celrep.2019.04.019.
880 59. Takatsuka, S., Yamada, H., Haniuda, K., Saruwatari, H., Ichihashi, M., Renauld, J.C.,
881 and Kitamura, D. (2018). IL-9 receptor signaling in memory B cells regulates humoral recall
882 responses. Nat Immunol *19*, 1025-1034. 10.1038/s41590-018-0177-0.
883 60. Rumfelt, L.L., Zhou, Y., Rowley, B.M., Shinton, S.A., and Hardy, R.R. (2006). Lineage
884 specification and plasticity in CD19- early B cell precursors. J Exp Med *203*, 675-687.
885 10.1084/jem.20052444.
886 61. Mallampati, S., Sun, B., Lu, Y., Ma, H., Gong, Y., Wang, D., Lee, J.S., Lin, K., and Sun,
887 X. (2014). Integrated genetic approaches identify the molecular mechanisms of Sox4 in early B-
888 cell development: intricate roles for RAG1/2 and CK1epsilon. Blood *123*, 4064-4076.
889 10.1182/blood-2013-12-543801.
890 62. Greig, K.T., de Graaf, C.A., Murphy, J.M., Carpinelli, M.R., Pang, S.H., Frampton, J.,
891 Kile, B.T., Hilton, D.J., and Nutt, S.L. (2010). Critical roles for c-Myb in lymphoid priming and
892 early B-cell development. Blood *115*, 2796-2805. 10.1182/blood-2009-08-239210.
893 63. Clark, M.R., Mandal, M., Ochiai, K., and Singh, H. (2014). Orchestrating B cell
894 lymphopoiesis through interplay of IL-7 receptor and pre-B cell receptor signalling. Nat Rev
895 Immunol *14*, 69-80. 10.1038/nri3570.
896 64. Callahan, D., Smita, S., Joachim, S., Hoehn, K., Kleinstein, S., Weisel, F., Chikina, M.,
897 and Shlomchik, M. (2024). Memory B cell subsets have divergent developmental origins that are

898 coupled to distinct imprinted epigenetic states. Nat Immunol *25*, 562-575. 10.1038/s41590-023-
899 01721-9.
900 65. Krishnamurty, A.T., Thouvenel, C.D., Portugal, S., Keitany, G.J., Kim, K.S., Holder, A.,
901 Crompton, P.D., Rawlings, D.J., and Pepper, M. (2016). Somatically Hypermutated
902 Plasmodium-Specific IgM(+) Memory B Cells Are Rapid, Plastic, Early Responders upon
903 Malaria Rechallenge. Immunity *45*, 402-414. 10.1016/j.immuni.2016.06.014.
904 66. Sutton, H.J., Aye, R., Idris, A.H., Vistein, R., Nduati, E., Kai, O., Mwacharo, J., Li, X.,
905 Gao, X., Andrews, T.D., et al. (2021). Atypical B cells are part of an alternative lineage of B cells
906 that participates in responses to vaccination and infection in humans. Cell Rep *34*, 108684.
907 10.1016/j.celrep.2020.108684.
908 67. Perez-Mazliah, D., Gardner, P.J., Schweighoffer, E., McLaughlin, S., Hosking, C.,
909 Tumwine, I., Davis, R.S., Potocnik, A.J., Tybulewicz, V.L., and Langhorne, J. (2018).
910 Plasmodium-specific atypical memory B cells are short-lived activated B cells. Elife *7*.
911 10.7554/eLife.39800.
912 68. Kikuchi, K., Kasai, H., Watanabe, A., Lai, A.Y., and Kondo, M. (2008). IL-7 specifies B
913 cell fate at the common lymphoid progenitor to pre-proB transition stage by maintaining early B
914 cell factor expression. Journal of immunology *181*, 383-392. 10.4049/jimmunol.181.1.383.
915 69. Corfe, S.A., and Paige, C.J. (2012). The many roles of IL-7 in B cell development;
916 mediator of survival, proliferation and differentiation. Semin Immunol *24*, 198-208.
917 10.1016/j.smim.2012.02.001.
918 70. Reya, T., O'Riordan, M., Okamura, R., Devaney, E., Willert, K., Nusse, R., and
919 Grosschedl, R. (2000). Wnt signaling regulates B lymphocyte proliferation through a LEF-1
920 dependent mechanism. Immunity *13*, 15-24. 10.1016/s1074-7613(00)00004-2.
921 71. Shehata, L., Thouvenel, C.D., Hondowicz, B.D., Pew, L.A., Pritchard, G.H., Rawlings,
922 D.J., Choi, J., and Pepper, M. (2024). Interleukin-4 downregulates transcription factor BCL6 to
923 promote memory B cell selection in germinal centers. Immunity *57*, 843-858 e845.
924 10.1016/j.immuni.2024.02.018.
925 72. Duan, L., Liu, D., Chen, H., Mintz, M.A., Chou, M.Y., Kotov, D.I., Xu, Y., An, J., Laidlaw,
926 B.J., and Cyster, J.G. (2021). Follicular dendritic cells restrict interleukin-4 availability in
927 germinal centers and foster memory B cell generation. Immunity *54*, 2256-2272 e2256.
928 10.1016/j.immuni.2021.08.028.
929 73. Ly, A., Liao, Y., Pietrzak, H., Ioannidis, L.J., Sidwell, T., Gloury, R., Doerflinger, M.,
930 Triglia, T., Qin, R.Z., Groom, J.R., et al. (2019). Transcription Factor T-bet in B Cells Modulates
931 Germinal Center Polarization and Antibody Affinity Maturation in Response to Malaria. Cell Rep
932 *29*, 2257-2269 e2256. 10.1016/j.celrep.2019.10.087.
933 74. Stone, S.L., Peel, J.N., Scharer, C.D., Risley, C.A., Chisolm, D.A., Schultz, M.D., Yu, B.,
934 Ballesteros-Tato, A., Wojciechowski, W., Mousseau, B., et al. (2019). T-bet Transcription Factor
935 Promotes Antibody-Secreting Cell Differentiation by Limiting the Inflammatory Effects of IFN-
936 gamma on B Cells. Immunity *50*, 1172-1187 e1177. 10.1016/j.immuni.2019.04.004.
937 75. Nellore, A., Zumaquero, E., Scharer, C.D., Fucile, C.F., Tipton, C.M., King, R.G., Mi, T.,
938 Mousseau, B., Bradley, J.E., Zhou, F., et al. (2023). A transcriptionally distinct subset of
939 influenza-specific effector memory B cells predicts long-lived antibody responses to vaccination
940 in humans. Immunity *56*, 847-863 e848. 10.1016/j.immuni.2023.03.001.
941 76. Curran, M.A., Geiger, T.L., Montalvo, W., Kim, M., Reiner, S.L., Al-Shamkhani, A., Sun,
942 J.C., and Allison, J.P. (2013). Systemic 4-1BB activation induces a novel T cell phenotype
943 driven by high expression of Eomesodermin. The Journal of experimental medicine *210*, 743-
944 755. 10.1084/jem.20121190.
945 77. Hong, J.P., Reynoso, G.V., Andhey, P.S., Swain, A., Turner, J.S., Boon, A.C.M.,
946 Krammer, F., Ellebedy, A.H., Zanini, F., Artyomov, M., et al. (2020). An Agonistic Anti-CD137

947 Antibody Disrupts Lymphoid Follicle Structure and T-Cell-Dependent Antibody Responses. Cell
948 Rep Med *1*. 10.1016/j.xcrm.2020.100035.
949 78. Racine, R., Jones, D.D., Chatterjee, M., McLaughlin, M., Macnamara, K.C., and
950 Winslow, G.M. (2010). Impaired germinal center responses and suppression of local IgG
951 production during intracellular bacterial infection. Journal of immunology *184*, 5085-5093.
952 10.4049/jimmunol.0902710.
953 79. Yates, J.L., Racine, R., McBride, K.M., and Winslow, G.M. (2013). T cell-dependent IgM
954 memory B cells generated during bacterial infection are required for IgG responses to antigen
955 challenge. Journal of immunology *191*, 1240-1249. 10.4049/jimmunol.1300062.
956 80. Moir, S., Ho, J., Malaspina, A., Wang, W., DiPoto, A.C., O'Shea, M.A., Roby, G., Kottilil,
957 S., Arthos, J., Proschan, M.A., et al. (2008). Evidence for HIV-associated B cell exhaustion in a
958 dysfunctional memory B cell compartment in HIV-infected viremic individuals. The Journal of
959 experimental medicine *205*, 1797-1805. 10.1084/jem.20072683.
960 81. Portugal, S., Tipton, C.M., Sohn, H., Kone, Y., Wang, J., Li, S., Skinner, J., Virtaneva, K.,
961 Sturdevant, D.E., Porcella, S.F., et al. (2015). Malaria-associated atypical memory B cells
962 exhibit markedly reduced B cell receptor signaling and effector function. Elife *4*.
963 10.7554/eLife.07218.
964 82. Sullivan, R.T., Kim, C.C., Fontana, M.F., Feeney, M.E., Jagannathan, P., Boyle, M.J.,
965 Drakeley, C.J., Ssewanyana, I., Nankya, F., Mayanja-Kizza, H., et al. (2015). FCRL5 Delineates
966 Functionally Impaired Memory B Cells Associated with Plasmodium falciparum Exposure. PLoS
967 Pathog *11*, e1004894. 10.1371/journal.ppat.1004894.
968 83. Elsner, R.A., Smita, S., and Shlomchik, M.J. (2024). IL-12 induces a B cell-intrinsic IL-
969 12/IFNgamma feed-forward loop promoting extrafollicular B cell responses. Nat Immunol *25*,
970 1283-1295. 10.1038/s41590-024-01858-1.
971 84. Kimura, T., Nakayama, K., Penninger, J., Kitagawa, M., Harada, H., Matsuyama, T.,
972 Tanaka, N., Kamijo, R., Vilcek, J., Mak, T.W., and et al. (1994). Involvement of the IRF-1
973 transcription factor in antiviral responses to interferons. Science *264*, 1921-1924.
974 10.1126/science.8009222.
975 85. Kim, I.K., Kim, B.S., Koh, C.H., Seok, J.W., Park, J.S., Shin, K.S., Bae, E.A., Lee, G.E.,
976 Jeon, H., Cho, J., et al. (2015). Glucocorticoid-induced tumor necrosis factor receptor-related
977 protein co-stimulation facilitates tumor regression by inducing IL-9-producing helper T cells. Nat
978 Med *21*, 1010-1017. 10.1038/nm.3922.
979 86. Niese, M.L., Pajulas, A.L., Rostron, C.R., Cheung, C.C.L., Krishnan, M.S., Zhang, J.,
980 Cannon, A.M., and Kaplan, M.H. (2024). TL1A priming induces a multi-cytokine Th9 cell
981 phenotype that promotes robust allergic inflammation in murine models of asthma. Mucosal
982 Immunol *17*, 537-553. 10.1016/j.mucimm.2024.03.006.
983 87. Ming, S., Zhang, M., Liang, Z., Li, C., He, J., Chen, P., Zhang, S., Niu, X., Deng, S.,
984 Geng, L., et al. (2021). OX40L/OX40 Signal Promotes IL-9 Production by Mucosal MAIT Cells
985 During Helicobacter pylori Infection. Front Immunol *12*, 626017. 10.3389/fimmu.2021.626017.
986 88. Xiao, X., Balasubramanian, S., Liu, W., Chu, X., Wang, H., Taparowsky, E.J., Fu, Y.X.,
987 Choi, Y., Walsh, M.C., and Li, X.C. (2012). OX40 signaling favors the induction of T(H)9 cells
988 and airway inflammation. Nat Immunol *13*, 981-990. 10.1038/ni.2390.
989 89. Shuford, W.W., Klussman, K., Tritchler, D.D., Loo, D.T., Chalupny, J., Siadak, A.W.,
990 Brown, T.J., Emswiler, J., Raecho, H., Larsen, C.P., et al. (1997). 4-1BB costimulatory signals
991 preferentially induce CD8+ T cell proliferation and lead to the amplification in vivo of cytotoxic T
992 cell responses. The Journal of experimental medicine *186*, 47-55. 10.1084/jem.186.1.47.
993 90. Tan, J.T., Whitmire, J.K., Murali-Krishna, K., Ahmed, R., Altman, J.D., Mittler, R.S.,
994 Sette, A., Pearson, T.C., and Larsen, C.P. (2000). 4-1BB costimulation is required for protective

995 anti-viral immunity after peptide vaccination. Journal of immunology *164*, 2320-2325.
996 10.4049/jimmunol.164.5.2320.
997 91. Wong, H.Y., Prasad, A., Gan, S.U., Chua, J.J.E., and Schwarz, H. (2020). Identification
998 of CD137-Expressing B Cells in Multiple Sclerosis Which Secrete IL-6 Upon Engagement by
999 CD137 Ligand. Front Immunol *11*, 571964. 10.3389/fimmu.2020.571964.
1000
1001

1002 **FIGURE LEGENDS**
1003
1004 **Fig. 1: Exogenous 4-1BB stimulation leads to loss of parasite control due to derailed GC**
1005 **response during *Plasmodium* infection. a,** Experimental design. C57BL/6 mice were infected
1006 with *Plasmodium yoelii*-parasitized red blood cells (*Py* pRBCs) and treated with 50μg of 4-1BB
1007 agonist antibody (3H3) or isotype control (rIgG) on days 5 and 7 post infection. **b**, Kinetics of
1008 parasite burden (% infected RBCs). Data are mean ± s.e.m and are pooled from *n=2* independent
1009 experiments using *n=7* mice for either group. **c,d,** Representative flow plots (left) and kinetics
1010 (right) of germinal center B cells (**c**) and germinal center Tfh cells (**d**) in the spleens of IgG- and
1011 3H3-treated mice. **e,** Summary graph of anti-MSP-1_{-19} IgG2b serum antibody end-point titers
1012 (EPT) on 21 and 39 dpi. For **c-e,** data are mean ± s.d and are representative of *n=2* biologically
1013 independent with similar results using *n=3* mice for either group. **f,** Confocal micrographs of rIgG-
1014 and 3H3-treated spleens on days 21 and 39 post infection showing total B cells (green), CD4 T
1015 cells (purple) and GC B cells (red). Data are representative of at least 2 biologically independent
1016 experiments. For **f**, scale bar: 200 μm. For **b, c** and **d,** two-way ANOVA and for **e,** two-tailed
1017 Students' *t* test was used for statistical analysis.
1018
1019 **Fig. 2: 4-1BB stimulation enhances MBC recall and protection against rechallenge**
1020 **independently of antigen load. a,** Experimental design. C57BL/6 mice were infected with *Py*
1021 and treated with 3H3 or isotype control as previously described. During the convalescent phase,
1022 mice were challenged with *Plasmodium berghei* ANKA-parasitized (*PbA*) RBCs. **b,** Survival graph
1023 of mice following *PbA* challenge. Data are pooled from two independent experiments. **c,** Fold
1024 change in anti-MSP-1_{-19} IgM serum antibody EPT between 0 and 5 dpi. Data are pairwise
1025 comparison of the two time points in each mouse and are pooled from *n=2* biologically
1026 independent experiments using *n=6* (rIgG) and *n=5* (3H3). **d,** Experimental design. C57BL/6 mice
1027 were infected with *Py* and treated with 3H3 or isotype control as previously described. Mice were
1028 treated with the Artemether (Artem) to control the parasite load and challenged with *PbA*. **e,**
1029 Survival of mice following *PbA* challenge. Data are pooled from two independent experiments. **f,**
1030 Fold change in anti-MSP-1_{-19} IgM serum antibody EPT between 0 and 5 dpi. Data represents
1031 pairwise comparison of the two time points in each mouse and are pooled from *n=2* biologically
1032 independent experiments with similar data using *n=7* (rIgG) and *n=7* (3H3). **g,** Experimental
1033 design. C57BL/6 mice were infected with irradiated parasites and treated with 3H3 or isotype
1034 control as previously described. During convalescence mice were rechallenged with *PbA*. **h,**
1035 Survival of mice following *PbA* infection. Data are pooled from two independent experiments. **i,**
1036 Fold change in anti-MSP-1_{-19} IgM serum antibody EPT between 0 and 5 dpi. Data are pairwise
1037 comparison of the two time points in each mouse and are pooled from *n=2* biologically
1038 independent experiments using *n=5* (rIgG) and *n=5* (3H3). For **b**, **e** and **h**, data were analyzed
1039 by Mantel-Cox test. For **c, f** and **i**, two-tailed Mann-Whitney U tests were used for statistical
1040 analysis.
1041
1042 **Fig. 3: Enhanced recall potential and not abundance of MBCs drives protection following**
1043 **4-1BB stimulation. a,** Anti-MSP-1_{-19} IgM ELISPOT of bone marrow plasma cells (BMPCs) on 5
1044 dpi post *PbA* challenge. Data are representative of *n=2* biologically independent experiments
1045 using *n=4* mice/group. **b-e**, *Py*-infected C57BL/6 mice were treated with 3H3 or isotype control as
1046 previously described. **d-f,** Mice were additionally treated with the antimalarial drug artemether at
1047 regular intervals as detailed elsewhere. Representative flow plots (left) and total numbers (right)
1048 of polyclonal (**b,d**) and MSP-1 specific (**c,e**) MBCs in the spleen. Data are either representative
1049 (**b,c**) or are pooled from *n=2* biologically independent experiments using *n=3-4* mice/group. **f,**

1050 Representative flow plots (left) and frequency (right) of proliferating BMPCs as detected by Ki67
1051 and TACI staining. **g,** Geometric mean fluorescence intensity (gMFI) of MSP-1 staining in MSP-
1052 1 specific MBCs. Data are representative of *n=2* biologically independent experiments using *n=3*
1053 mice/group. **h,** Total MBCs from rIgG- and 3H3-treated mice were flow-sorted and transferred to
1054 μMT recipients that were infected with *Py* the following day. **h**, Summary graphs showing parasite
1055 burden on 12 dpi and **i**, anti-MSP-1_{-19} IgM serum antibody titers on 4 dpi. Data are representative
1056 of *n=2* biologically independent experiments using *n=4* mice/group. Data were analyzed by two-
1057 tailed Mann-Whitney U tests (**a-e** and **g-l)**, and Student's *t* test (**f**).
1058
1059 **Fig. 4: Exogenous 4-1BB ligation induces MBCs with an extrafollicular gene signature. a,**
1060 Experimental design. C57BL/6 mice were infected and treated as indicated. Polyclonal and MSP-
1061 1 specific MBCs were flow-sorted and scRNA-seq, V(D)J sequencing and CITE-seq were
1062 performed. **b,** UMAP showing the identified clusters of polyclonal MBCs. **c,** Pie diagram depicting
1063 the frequency of respective clusters in the polyclonal MBC pool derived from rIgG and 3H3-treated
1064 mice. **d,** Heatmap depicting markers from each cluster with selected genes highlighted on the left.
1065 **e,f,** Cells were scored based on gene signatures of MBCs derived from a GC response, EF
1066 response or from atypical B cells and were visualized per cluster (**e**) and the prevalence of each
1067 of these signatures are compared between treatments as shown (**f**). **g,** UMAP showing clusters
1068 in MSP-1 specific MBCs. **h,** Frequency of clusters in MSP-1 specific MBCs from rIgG or 3H3-
1069 treated mice cells are shown in the pie chart. **i,** Heatmap of markers from each cluster with
1070 selected genes highlighted on the left. **j,k,** Cells were scored based on gene signatures of MBCs
1071 derived from a GC response, EF response or atypical B cells and visualized per cluster (**j**) and
1072 between treatments (**k**). Data from **f** and **k** were analyzed by Wilcoxon test. Cells were pooled
1073 from 3 mice per group prior to sequencing.
1074
1075 **Fig. 5: 4-1BB stimulation skews MBC differentiation towards a highly functional**
1076 **population.** C57BL/6 mice were infected and treated as indicated in **Fig. 4a**. Distribution of IgM
1077 (**a**), CD73 and CD80 (**b**) expression among the polyclonal MBCs clusters. **c,** Pseudo time
1078 trajectories (left) and their representative contributions towards each cluster in polyclonal MBCs
1079 in rIgG- and 3H3-treated mice (right) based on their frequencies in **Fig. 4c**. Distribution of IgM (**d**),
1080 CD73 and CD80 (**e**) expression among the MSP-1 specific MBCs clusters. **f,** Pseudo time
1081 trajectories (left) and their representative contributions in MSP-1 specific MBCs in rIgG- and 3H3-
1082 treated mice (right) based on their frequencies in **Fig. 4h**. Gene ontology (GO) analysis of
1083 upregulated genes in MBCs from 3H3-treated mice compared to MBCs from rIgG-treated mice in
1084 clusters 0 and 2 of polyclonal MBCs combined (**g**) and cluster 1 of MSP-1 specific MBCs (**h**).
1085
1086 **Fig. 6: 3H3-driven protection is dependent on IL-9:IL-9R signaling.** C57BL/6 mice were
1087 infected and treated as indicated in **Fig. 4a**. UMAP clustering of scRNA-seq data showing *Il9r*
1088 expression among polyclonal (**a**) and MSP-1 specific MBC clusters (**b**). **c,** UMAP clustering of
1089 polyclonal MBCs on 38 dpi generated by FlowSOM. **d,** Expression levels of various proteins using
1090 FlowSOM clustering of polyclonal MBCs. **e,** Geometric mean fluorescence intensity (gMFI) of IL-
1091 9R in polyclonal MBCs on 38 dpi. Data is pooled from *n=2* biologically independent experiments
1092 using n=4 mice/group/experiment. **f,** UMAP clustering of MSP-1 specific MBCs on 38 dpi
1093 generated by FlowSOM. **g,** Expression levels of various proteins using FlowSOM clustering of
1094 MSP-1 specific MBCs. **h,** gMFI of IL-9R in MSP-1 specific MBCs on 38 dpi. Data is pooled from
1095 *n=2* biologically independent experiments using n=4 mice/group/experiment. **i,j,** WT mice were
1096 infected with *Py* and treated with rIgG or 3H3 and then with the antimalarial drug artemether at
1097 regular intervals. One day prior and after *PbA* rechallenge, mice were treated with αIL-9
1098 neutralizing antibody or isotype control (mIgG) (as detailed in **Supp Fig. 7d**). Survival was

monitored (**i**) and fold change in anti-MSP-1_{-19} IgM serum antibody EPT between 0 and 5 dpi was assessed (**j**). Data is pooled from *n=2* biologically independent experiments using *n=6* mice/group. **k**,**l,** B cell-specific WT (B^{WT}) and IL-9R KO ($B^{IL\text{-}9R\ KO}$) chimeras generated and were infected with *Py* and treated with 3H3 on days 5 and 7 post infection and then with the antimalarial drug artemether at regular intervals (**Supp Fig.7e**). On 38 dpi, during the convalescent phase, mice were rechallenged with *PbA*. Survival was monitored (**k**) and fold change in anti-MSP-1_{-19} IgM serum antibody EPT between 0 and 5 dpi was assessed (**l**). Data is pooled from *n=2* biologically independent experiments using *n=11* mice/group (**k**) and are representative of *n=2* biologically independent experiments using *n=5-6* mice/group (**l**). For **e**, **h**, **j** and **l** two-tailed Mann-Whitney U tests were used for statistical analysis. For **i** and **k**, data were analyzed by Mantel-Cox.

Fig. 7: Altered chromatin landscape in MBCs following 4-1BB stimulation poises them to readily become PCs upon recall. a, Experimental design. C57BL/6 mice were infected and treated as indicated. Polyclonal and MSP-1 specific MBCs were flow-sorted and scATAC-seq was performed. **b,** UMAP clustering of MSP-1 specific MBCs using scATAC-seq data with transferred labels from scRNA-seq post data integration. Comparison of *Il9r* (**c**) and *Prdm1* (**d**) accessibility between clusters 0 and 1 of MSP-1 specific MBCs. **e,** Motif analysis of differentially accessible regions (DARs) in cluster 1 of MSP-1 specific MBCs compared to the other clusters. **f,** Comparison of *Il9r* accessibility in cluster 1 between MSP-1 specific MBCs obtained from rIgG and 3H3-treated mice. **g,** Motif analysis of differentially accessible regions (DARs) in 3H3 compared to rIgG in cluster 1 of MSP-1 specific MBCs. Sequenced nuclei were pooled from 4 mice per group.

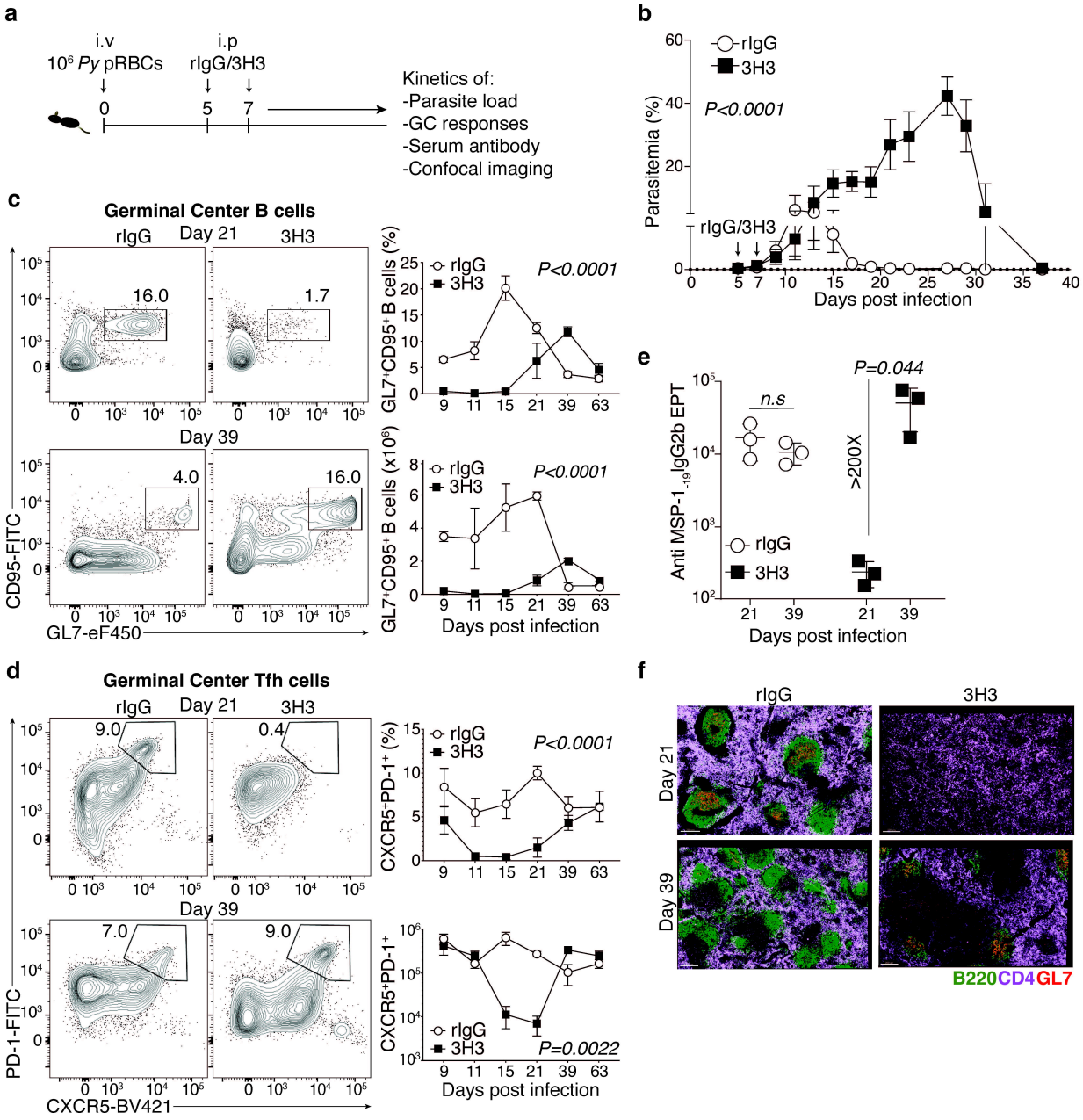
a
i.v
10⁶ Py pRBCs
i.p
rIgG/3H3
0
5
7
Kinetics of:
-Parasite load
-GC responses
-Serum antibody
-Confocal imaging
b
rIgG
3H3
P<0.0001
Parasitemia (%)
rIgG/3H3
Days post infection
c
Germinal Center B cells
rIgG
Day 21
3H3
16.0
1.7
Day 39
4.0
16.0
CD95-FITC
GL7-eF450
GL7+CD95+ B cells (%)
P<0.0001
GL7+CD95+ B cells (x10⁶)
P<0.0001
Days post infection
e
P=0.044
n.s
>200X
Anti MSP-1-19 IgG2b EPT
rIgG
3H3
Days post infection
d
Germinal Center Tfh cells
rIgG
Day 21
3H3
9.0
0.4
Day 39
7.0
9.0
PD-1-FITC
CXCR5-BV421
CXCR5+PD-1+ (%)
P<0.0001
CXCR5+PD-1+
P=0.0022
Days post infection
f
rIgG
3H3
Day 21
Day 39
B220CD4GL7

Figure 2

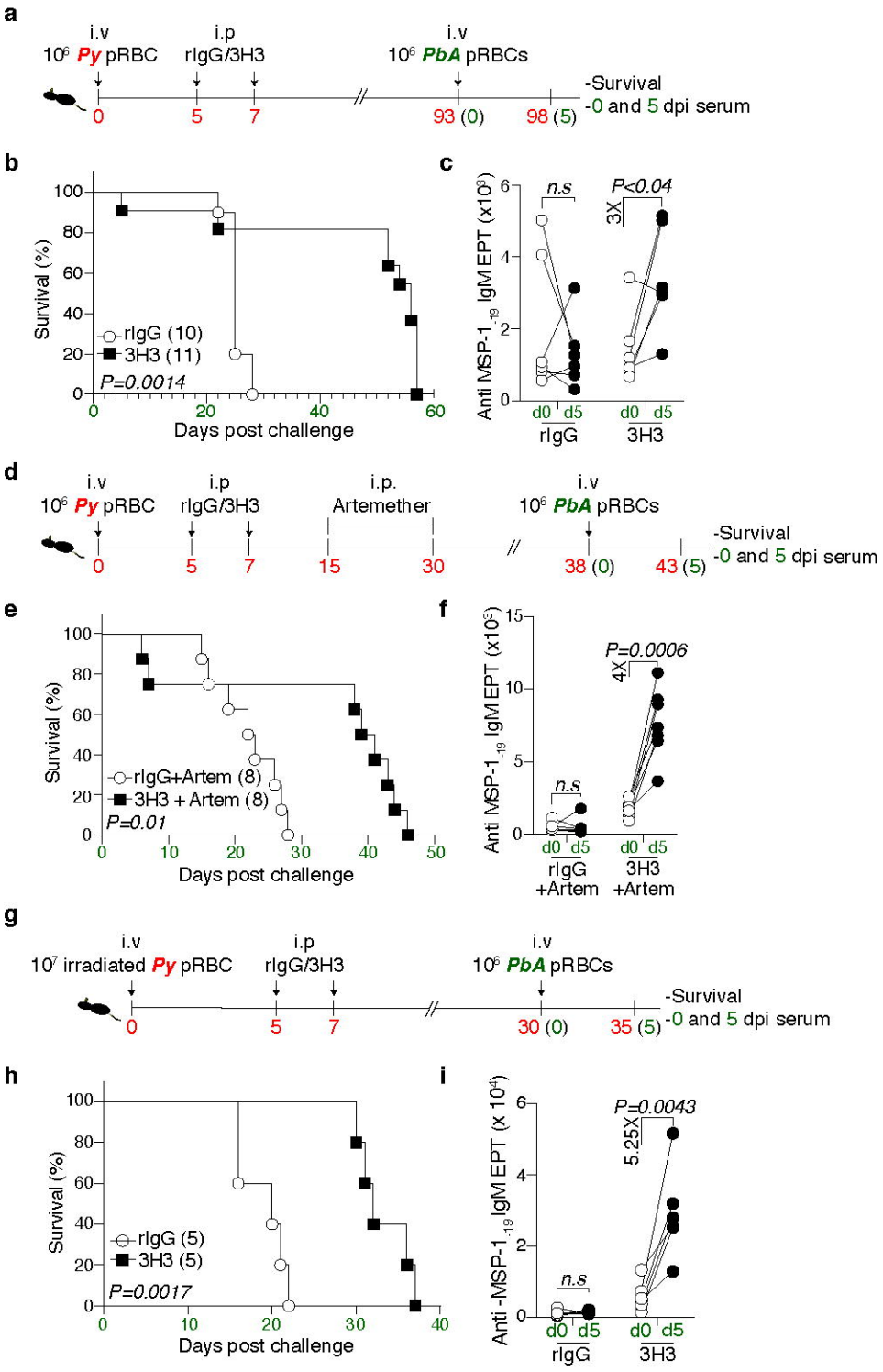
a
i.v
10^6 Py pRBC
i.p
rIgG/3H3
i.v
10^6 PbA pRBCs
-Survival
-0 and 5 dpi serum
0
5
7
93 (0)
98 (5)
b
Survival (%)
rIgG (10)
3H3 (11)
P=0.0014
Days post challenge
c
Anti MSP-1-19 IgM EPT (x10^3)
n.s
P<0.04
3X
d0 d5
rIgG
3H3
d
i.v
10^6 Py pRBC
i.p
rIgG/3H3
i.p.
Artemether
i.v
10^6 PbA pRBCs
-Survival
-0 and 5 dpi serum
0
5
7
15
30
38 (0)
43 (5)
e
Survival (%)
rIgG+Artem (8)
3H3 + Artem (8)
P=0.01
Days post challenge
f
Anti MSP-1-19 IgM EPT (x10^3)
P=0.0006
4X
n.s
d0 d5
rIgG +Artem
3H3 +Artem
g
i.v
10^7 irradiated Py pRBC
i.p
rIgG/3H3
i.v
10^6 PbA pRBCs
-Survival
-0 and 5 dpi serum
0
5
7
30 (0)
35 (5)
h
Survival (%)
rIgG (5)
3H3 (5)
P=0.0017
Days post challenge
i
Anti -MSP-1-19 IgM EPT (x 10^3)
P=0.0043
5.25X
n.s
d0 d5
rIgG
3H3

Figure 3

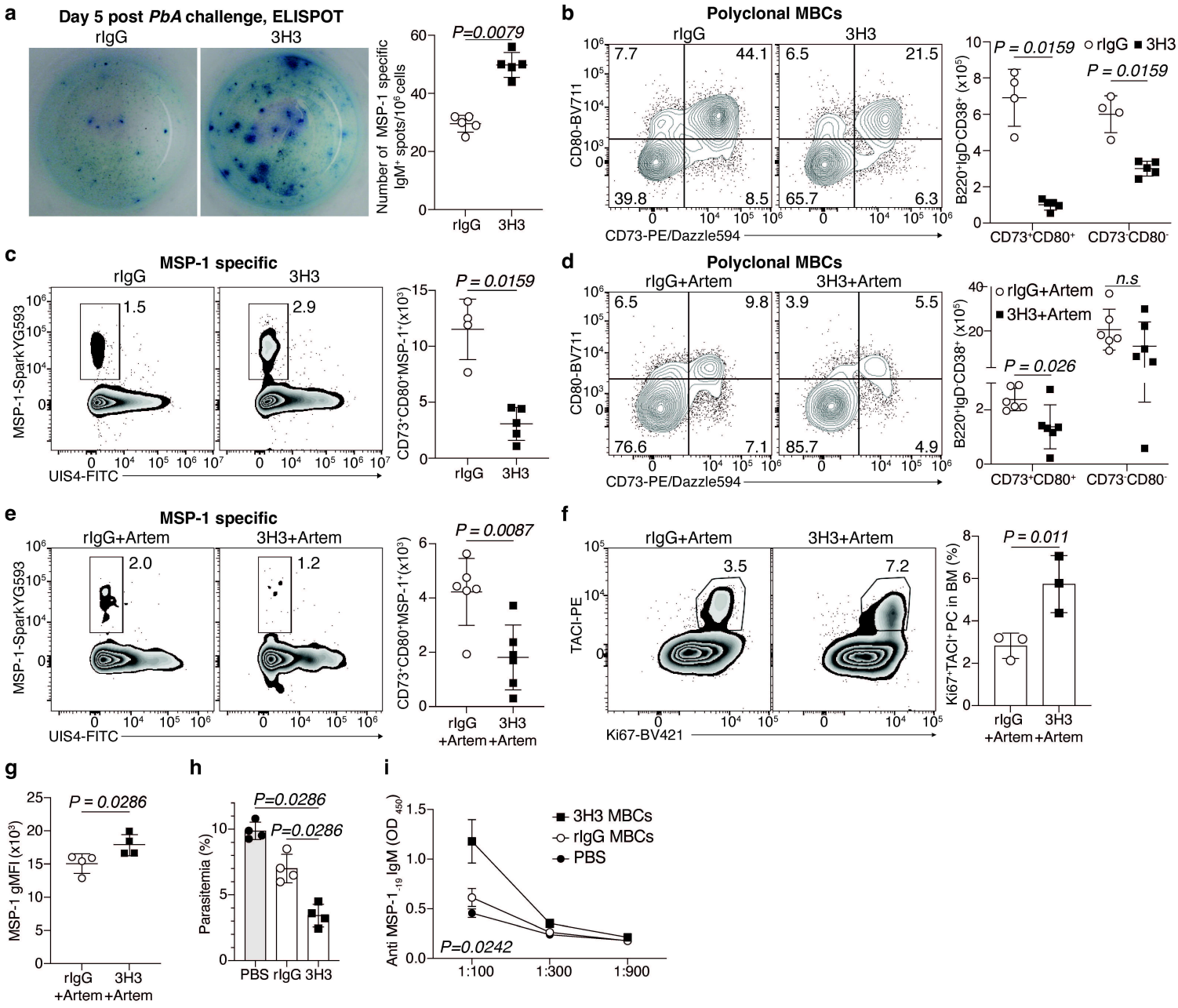
a
Day 5 post PbA challenge, ELISPOT
rIgG
3H3
P=0.0079
Number of MSP-1 specific IgM+ spots/10^6 cells
b
Polyclonal MBCs
rIgG
3H3
7.7
44.1
39.8
8.5
6.5
21.5
65.7
6.3
CD80-BV711
CD73-PE/Dazzle594
P = 0.0159
P = 0.0159
rIgG 3H3
B220+IgD-CD38+ (x10^5)
CD73+CD80+
CD73-CD80-
c
MSP-1 specific
rIgG
3H3
1.5
2.9
MSP-1-SparkYG593
UIS4-FITC
P = 0.0159
CD73+CD80+MSP-1+(x10^3)
d
Polyclonal MBCs
rIgG+Artem
3H3+Artem
6.5
9.8
76.6
7.1
3.9
5.5
85.7
4.9
CD80-BV711
CD73-PE/Dazzle594
rIgG+Artem
3H3+Artem
n.s
P = 0.026
B220+IgD-CD38+ (x10^5)
CD73+CD80+
CD73-CD80-
e
MSP-1 specific
rIgG+Artem
3H3+Artem
2.0
1.2
MSP-1-SparkYG593
UIS4-FITC
P = 0.0087
CD73+CD80+MSP-1+(x10^3)
rIgG +Artem
3H3 +Artem
f
rIgG+Artem
3H3+Artem
3.5
7.2
TACI-PE
Ki67-BV421
P = 0.011
Ki67+TACI+ PC in BM (%)
rIgG +Artem
3H3 +Artem
g
P = 0.0286
MSP-1 gMFI (x10^3)
rIgG +Artem
3H3 +Artem
h
P=0.0286
P=0.0286
Parasitemia (%)
PBS rIgG 3H3
i
3H3 MBCs
rIgG MBCs
PBS
P=0.0242
Anti MSP-1-19 IgM (OD 450)
1:100
1:300
1:900

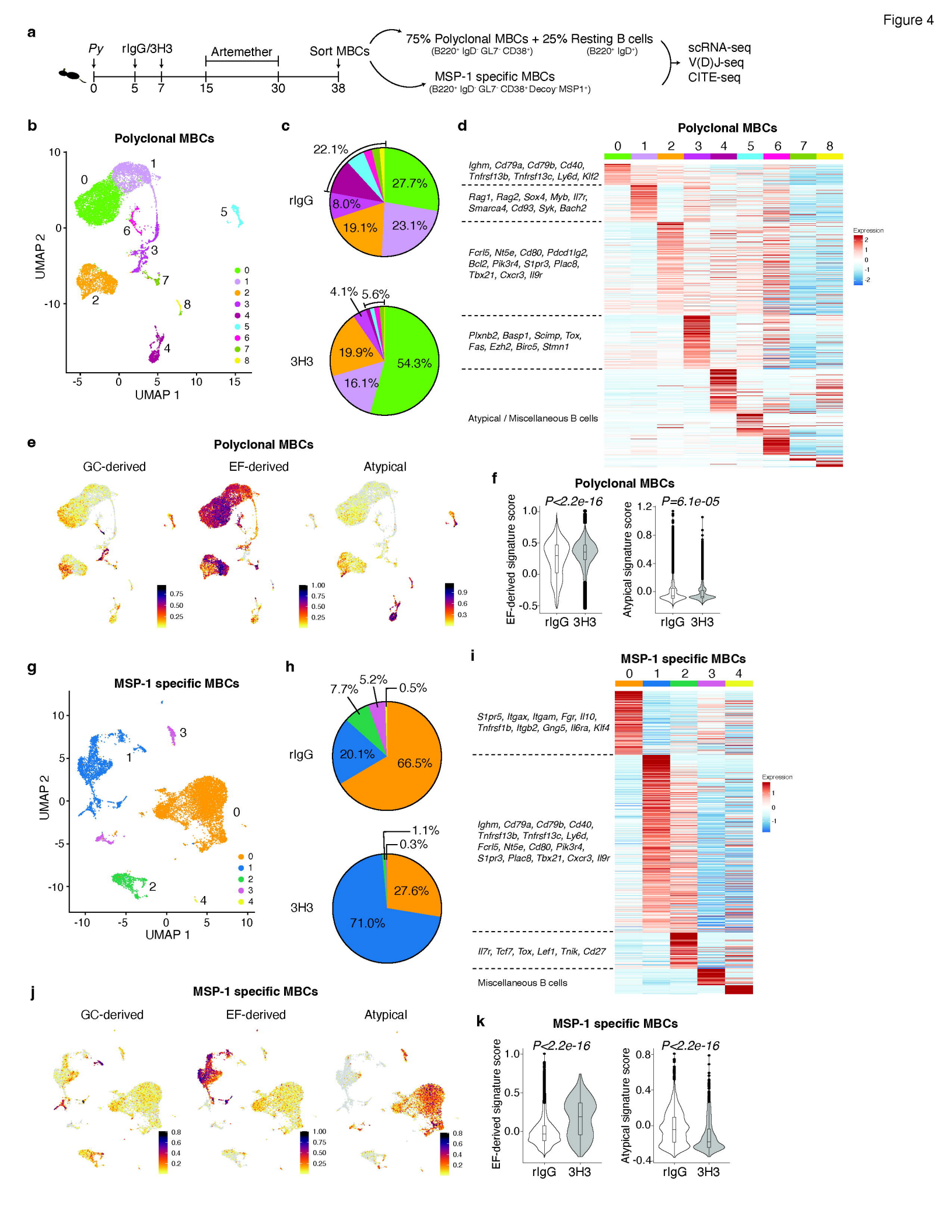
a
Py
rIgG/3H3
Artemether
Sort MBCs
0
5
7
15
30
38
75% Polyclonal MBCs + 25% Resting B cells
(B220+ IgD- GL7- CD38+)
(B220+ IgD+)
MSP-1 specific MBCs
(B220+ IgD- GL7- CD38+ Decoy- MSP1+)
scRNA-seq
V(D)J-seq
CITE-seq
b
Polyclonal MBCs
UMAP 2
UMAP 1
c
rIgG
22.1%
27.7%
8.0%
19.1%
23.1%
3H3
4.1%
5.6%
19.9%
54.3%
16.1%
d
Polyclonal MBCs
Ighm, Cd79a, Cd79b, Cd40, Tnfrsf13b, Tnfrsf13c, Ly6d, Klf2
Rag1, Rag2, Sox4, Myb, Il7r, Smarca4, Cd93, Syk, Bach2
Fcrl5, Nt5e, Cd80, Pdcd1lg2, Bcl2, Pik3r4, S1pr3, Plac8, Tbx21, Cxcr3, Il9r
Plxnb2, Basp1, Scimp, Tox, Fas, Ezh2, Birc5, Stmn1
Atypical / Miscellaneous B cells
Expression
e
Polyclonal MBCs
GC-derived
EF-derived
Atypical
f
Polyclonal MBCs
P<2.2e-16
P=6.1e-05
EF-derived signature score
Atypical signature score
rIgG
3H3
g
MSP-1 specific MBCs
UMAP 2
UMAP 1
h
rIgG
7.7%
5.2%
0.5%
20.1%
66.5%
3H3
1.1%
0.3%
27.6%
71.0%
i
MSP-1 specific MBCs
S1pr5, Itgax, Itgam, Fgr, Il10, Tnfrsf1b, Itgb2, Gng5, Il6ra, Klf4
Ighm, Cd79a, Cd79b, Cd40, Tnfrsf13b, Tnfrsf13c, Ly6d, Fcrl5, Nt5e, Cd80, Pik3r4, S1pr3, Plac8, Tbx21, Cxcr3, Il9r
Il7r, Tcf7, Tox, Lef1, Tnik, Cd27
Miscellaneous B cells
Expression
j
MSP-1 specific MBCs
GC-derived
EF-derived
Atypical
k
MSP-1 specific MBCs
P<2.2e-16
P<2.2e-16
EF-derived signature score
Atypical signature score
rIgG
3H3

Figure 5

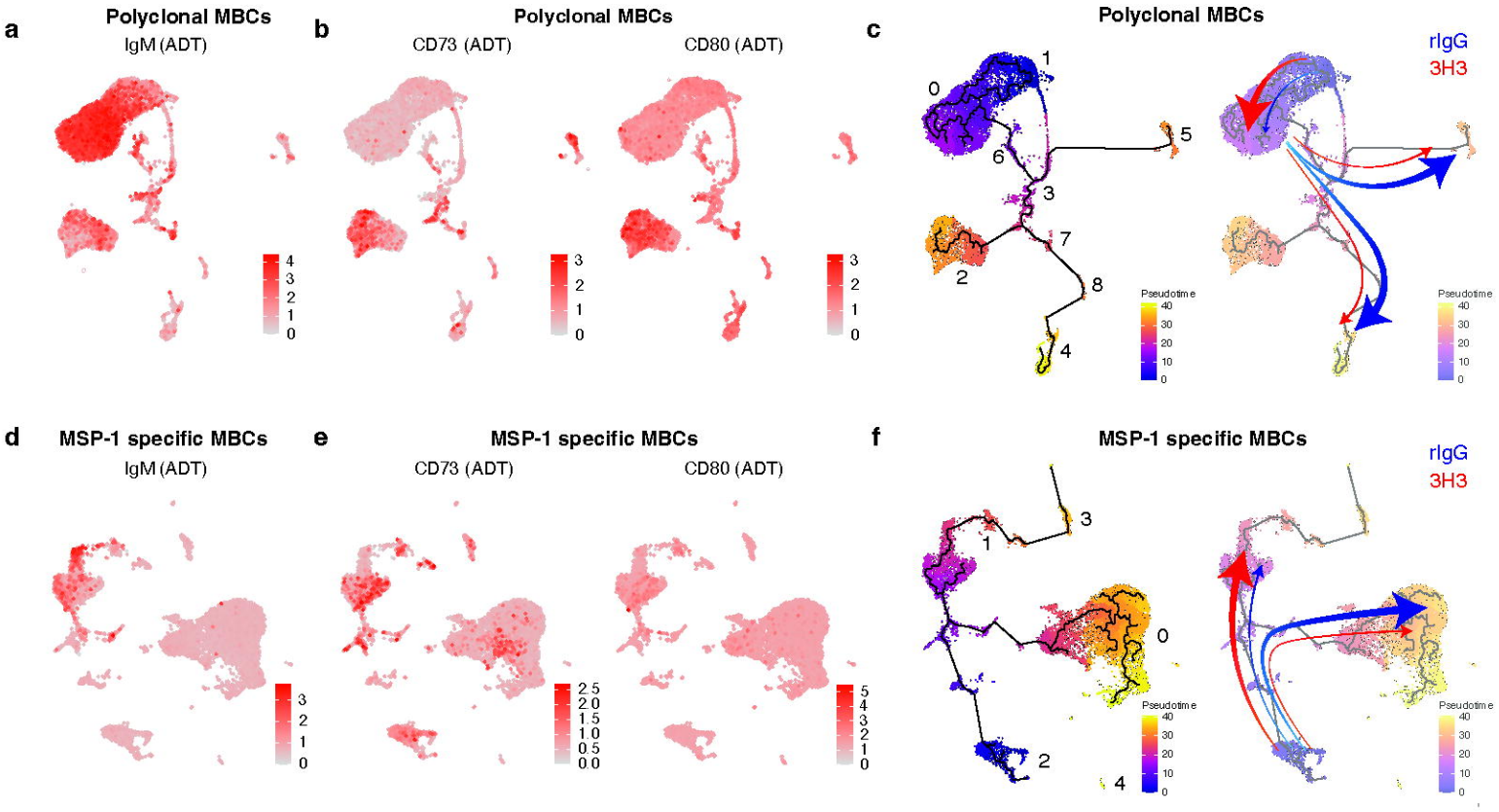
a
Polyclonal MBCs
IgM (ADT)
b
Polyclonal MBCs
CD73 (ADT)
CD80 (ADT)
c
Polyclonal MBCs
rIgG
3H3
Pseudotime
d
MSP-1 specific MBCs
IgM (ADT)
e
MSP-1 specific MBCs
CD73 (ADT)
CD80 (ADT)
f
MSP-1 specific MBCs
rIgG
3H3
Pseudotime

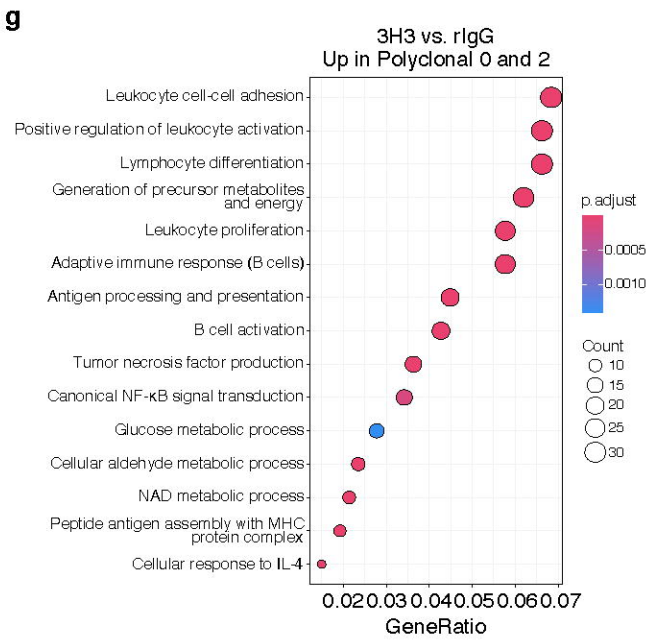
g
3H3 vs. rIgG
Up in Polyclonal 0 and 2
Leukocyte cell-cell adhesion
Positive regulation of leukocyte activation
Lymphocyte differentiation
Generation of precursor metabolites and energy
Leukocyte proliferation
Adaptive immune response (B cells)
Antigen processing and presentation
B cell activation
Tumor necrosis factor production
Canonical NF-κB signal transduction
Glucose metabolic process
Cellular aldehyde metabolic process
NAD metabolic process
Peptide antigen assembly with MHC protein complex
Cellular response to IL-4
p.adjust
Count
GeneRatio

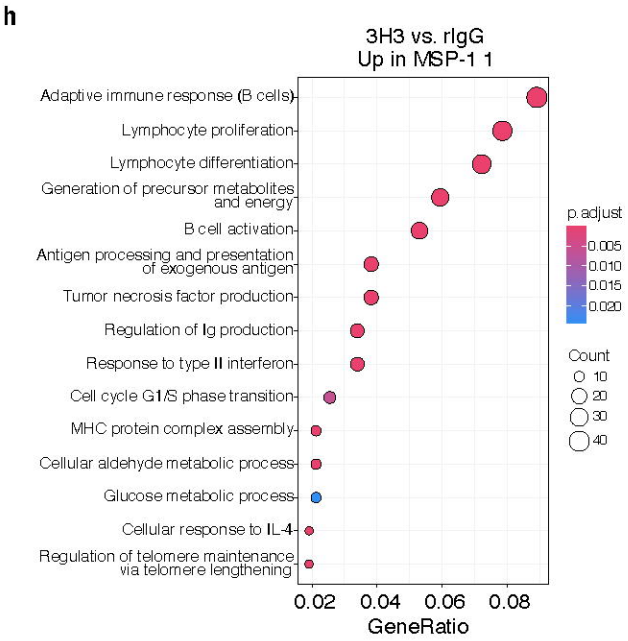
h
3H3 vs. rIgG
Up in MSP-1 1
Adaptive immune response (B cells)
Lymphocyte proliferation
Lymphocyte differentiation
Generation of precursor metabolites and energy
B cell activation
Antigen processing and presentation of exogenous antigen
Tumor necrosis factor production
Regulation of Ig production
Response to type II interferon
Cell cycle G1/S phase transition
MHC protein complex assembly
Cellular aldehyde metabolic process
Glucose metabolic process
Cellular response to IL-4
Regulation of telomere maintenance via telomere lengthening
p.adjust
Count
GeneRatio

Figure 6

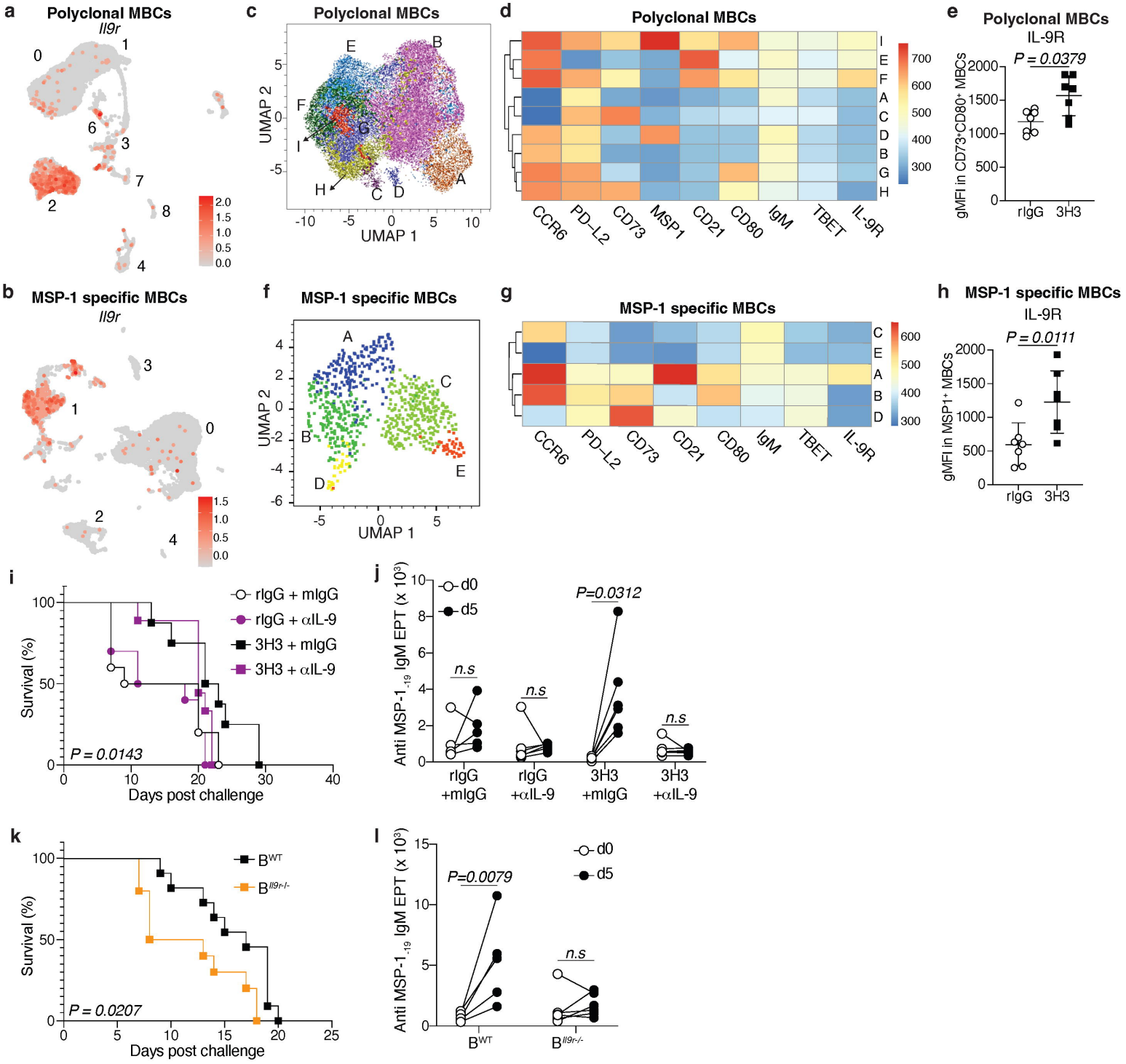
a
Polyclonal MBCs
Il9r
b
MSP-1 specific MBCs
Il9r
c
Polyclonal MBCs
UMAP 1
UMAP 2
d
Polyclonal MBCs
CCR6
PD-L2
CD73
MSP1
CD21
CD80
IgM
TBET
IL-9R
e
Polyclonal MBCs
IL-9R
P = 0.0379
gMFI in CD73+CD80+ MBCs
rIgG
3H3
f
MSP-1 specific MBCs
UMAP 1
UMAP 2
g
MSP-1 specific MBCs
h
MSP-1 specific MBCs
IL-9R
P = 0.0111
gMFI in MSP1+ MBCs
i
rIgG + mIgG
rIgG + αIL-9
3H3 + mIgG
3H3 + αIL-9
Survival (%)
P = 0.0143
Days post challenge
j
d0
d5
P=0.0312
n.s
Anti MSP-1-19 IgM EPT (x 10³)
rIgG +mIgG
rIgG +αIL-9
3H3 +mIgG
3H3 +αIL-9
k
BWT
BIl9r-/-
Survival (%)
P = 0.0207
Days post challenge
l
d0
d5
P=0.0079
n.s
Anti MSP-1-19 IgM EPT (x 10³)
BWT
BIl9r-/-

Figure 7

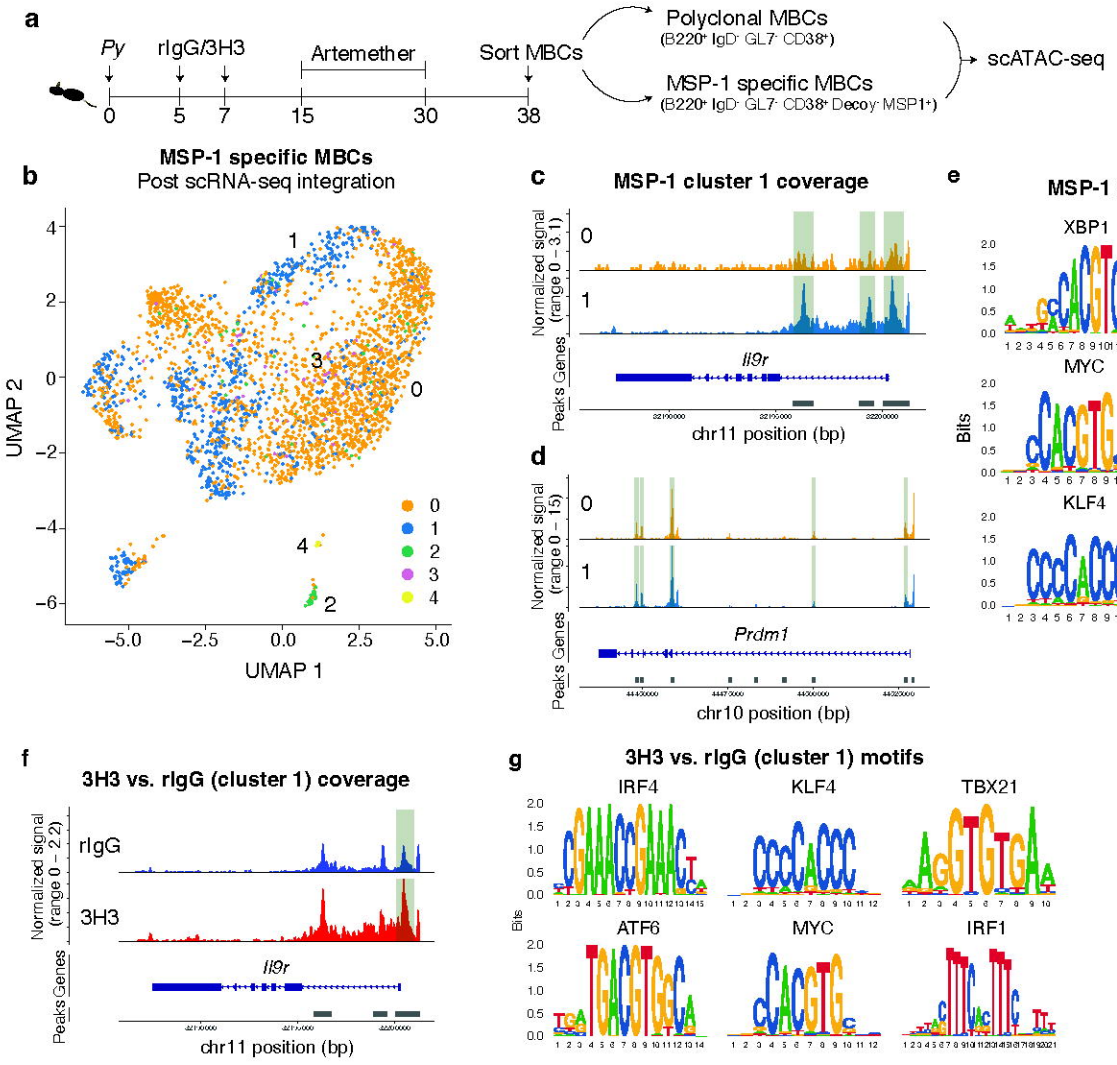
a
Py
rIgG/3H3
Artemether
Sort MBCs
0
5
7
15
30
38
Polyclonal MBCs
(B220+ IgD- GL7- CD38+)
MSP-1 specific MBCs
(B220+ IgD- GL7- CD38+ Decoy- MSP1+)
scATAC-seq
b
MSP-1 specific MBCs
Post scRNA-seq integration
UMAP 2
UMAP 1
c
MSP-1 cluster 1 coverage
Normalized signal (range 0 – 3.1)
Peaks Genes
Il9r
chr11 position (bp)
d
Normalized signal (range 0 – 15)
Prdm1
chr10 position (bp)
e
MSP-1 cluster 1 motifs
XBP1
ATF3
MYC
ATF6
KLF4
BHLHE40
Bits
f
3H3 vs. rIgG (cluster 1) coverage
rIgG
3H3
Normalized signal (range 0 – 2.2)
Peaks Genes
Il9r
chr11 position (bp)
g
3H3 vs. rIgG (cluster 1) motifs
IRF4
KLF4
TBX21
ATF6
MYC
IRF1
Bits